R. & M. No. 3381

MINISTRY OF AVIATION

AERONAUTICAL RESEARCH COUNCIL
REPORTS AND MEMORANDA

Measurements of Aerodynamic Derivatives on a Wing with a Series of Tip Bodies

By P. R. GUYETT

LONDON: HER MAJESTY'S STATIONERY OFFICE
1964
PRICE £1 0s. 0d. NET

Measurements of Aerodynamic Derivatives on a Wing with a Series of Tip Bodies

By P. R. GUYETT

COMMUNICATED BY THE DEPUTY CONTROLLER AIRCRAFT (RESEARCH AND DEVELOPMENT)
MINISTRY OF AVIATION

*Reports and Memoranda No. 3381**
March, 1963

Summary.

Oscillatory aerodynamic lift and pitching-moment derivatives have been measured in a wind tunnel at low subsonic speeds on the following wing and wing-body combinations:

(i) tapered wing of aspect ratio 1·3, mid-chord line unswept, with a sharp leading edge,

(ii) above wing fitted with a nacelle in three chordwise positions at the tip,

(iii) wing at (i) fitted with a tip body representing a tank or store, and tested with and without a fin at the rear of the body.

The measured derivatives for the wing alone are in good agreement with values calculated using lifting-surface theory, and are in reasonable agreement with values calculated using a semi-empirical method.

Derivatives for the wing with nacelle in the central position have been calculated using a semi-empirical method which makes an allowance for aerodynamic interference effects, and comparison shows that the values are reasonably accurate.

LIST OF CONTENTS

* Replaces R.A.E. Report No. Structures 285—A.R.C. 24 939.

LIST OF CONTENTS—*continued*

LIST OF APPENDICES

LIST OF TABLES

LIST OF ILLUSTRATIONS

---

1. *Introduction.*

There is a good deal of evidence that existing theoretical methods can predict with accuracy the aerodynamic forces acting on surfaces oscillating with attached flow at low subsonic wind speeds. For sections with sharp leading edges, however, and also for surfaces of low aspect ratio with blunt streamwise tips, separation of the flow occurs at small angles of attack, and the aerodynamic forces are then not linearly proportional to incidence. In these conditions the accuracy of the theoretical linearised results is in doubt and experimental information is required to resolve this uncertainty.

This report describes measurements of aerodynamic derivatives on a nominally unswept straight-tapered wing of low aspect ratio with a sharp leading edge. Tests were made for amplitudes of oscillation in pitch of $\pm 2\frac{1}{2}°$ and $\pm 5°$ about a mean angle of attack of 0°. The results show that although the values of the derivatives depend upon the amplitude, the variation is fairly small in the test range, and that the conventional theoretical methods give a good indication of the values of the derivatives.

A second problem of current interest is the estimation of derivatives for surfaces with bodies at the tips which introduce significant aerodynamic interference. Theoretical solutions have not yet been determined for this general configuration in unsteady flow, and the analysis clearly presents considerable difficulty. Measured values of derivatives are given in this report for the low-aspect-ratio surface described above fitted with a series of tip bodies. These results indicate the importance of the aerodynamic interference effects, and also provide experimental data to assess the accuracy of methods for predicting their magnitude. Some values of derivatives found using a semi-empirical approach are shown to be in fairly good agreement with the measured results. A description of the semi-empirical method is included.

2. *Method.*

A half-span model wing was mounted vertically in a wind tunnel, and aerodynamic derivatives for pitch and normal translation were found by measuring the lift and moment during sustained pitching oscillations about two spanwise axis positions. The lift and pitching moment were determined from the output of a force transducer in a linkage providing the excitation about the axis, and from the output of a force transducer measuring the lift at the axis.

In each mode of oscillation the reactions of the inertia forces at the force measuring points were reduced by mounting the wing on a set of earthed springs. The springs were arranged to give a balance between the stiffness and inertia forces at a chosen frequency of oscillation, and this frequency was maintained throughout the tests. Frequency parameter was varied by altering the wind speed.

The method of calculating the required spring stiffnesses and positions has been described in detail in Ref. 1. When a precise balance of stiffness and inertia force is obtained, the forces measured in an oscillation in still air at the chosen frequency arise solely from the still-air aerodynamic damping and the apparatus damping. If the wing is then oscillated in a windstream at the same frequency and amplitude the additional forces measured, which in general are large compared with the still-air forces, give directly the additional aerodynamic forces acting on the wing.

3. *Apparatus.*

3.1. *Wind Tunnel.*

The tests were made in the Royal Aircraft Establishment 5 ft diameter Low-Speed Wind Tunnel. The working section was closed for these tests by fitting a circular-section tube between the entry nozzle and the safety screen. A fairing was added to the bottom of the tube to give a horizontal flat surface at the model position.

3.2. *Wing and Support.*

The half-span model wing was supported through a slot in the fairing at the bottom of the circular tube in the working section of the wind tunnel. To reduce the air flow through this slot and around the wing root a plywood plate was fixed to the wing and oscillated with it. In addition wooden strips were fitted on the fairing around the plate to form a shallow well. Figs. 1 and 2 show the position of the model in the tunnel. The horizontal flat surfaces normal to the wing at its root were considered to act as a reflector plate to simulate symmetrical aerodynamic loading.

Dimensions of the wing are given in Fig. 3. The wing was of straight-tapered planform, with a ratio of tip chord to root chord of 0·538, and leading-edge sweepback 26°. The mean chord was 1·487 ft. The geometric aspect ratio of the half-span wing was 0·638, equivalent to a full-span aspect ratio of 1·276. In section the wing profile was symmetrical, the streamwise profile being straight from the leading edge to 0·36 of the chord, and straight from 0·66 of the chord to the trailing edge, with a parabolic arc in the centre fitted tangentially to these lines, giving a ratio of thickness to chord of 0·034. The leading edge was rounded to a constant radius of 0·003 inches, and the trailing edge was blunt, of thickness 0·002 of the local chord.

Dimensions of the tip bodies, comprising a nacelle and a tank, are given in Fig. 4. The nacelle was basically rectangular in section with the corners rounded to a radius of 0·74 inches. The maximum spanwise dimension was 2·932 inches, and the maximum depth 3·070 inches. The overall length of the nacelle was 16 inches, equal to 0·894 of the plain-wing mean chord. The nacelle was hollowed to allow some flow through. Tests were made with the nacelle in three chordwise positions at the wing tip (*see* Fig. 5): in the central position the rear of the nacelle was behind the wing leading edge at the tip by a distance equal to 0·703 of the mean chord, in the forward position the corresponding distance was 0·516 of the mean chord, in the rear position the distance was 0·895 of the mean chord.

The tank was circular in cross-section, the local radius being determined from the ordinates of the RAE 104 aerofoil scaled to make the ratio of the maximum radius to the length of the tank 0·083. The overall length of the tank was 18 inches, equal to 1·009 of the plain-wing mean chord, and it was mounted at the wing tip with its nose projecting ahead of the wing leading edge by a distance equal to 0·168 of the mean chord (Fig. 5). The tank rear fin was straight tapered in planform with a nominal root chord of 4 inches at the tank centre-line, a tip chord of 2 inches and a length of 3 inches.

The wing was solid and constructed of light alloy with an integral root block. The nacelle was made of mahogany, and the tank of solid spruce. The fin was cut from 16 s.w.g. (0·064 inches thickness) light alloy sheet with chamfered leading and trailing edges, and bolted into a slot in the rear of the tank. The nacelle and tank were attached to the wing by screws connecting with a tongue fitted at the wing tip.

The wing was supported by light alloy brackets bolted to the front and the rear of the wing-root block. A steel channel was attached to either the front or the rear bracket and carried a cross-spring bearing unit forming the pitching axis. The cross-spring bearing was bolted to a rectangular welded frame which in turn was attached to a further cross-spring bearing unit bolted to a vertical member in a heavy base frame. Fig. 1 shows the arrangement for wing pitch about the rear axis. A force transducer was connected between the base and the rectangular frame close to the pitching axis. The output of this transducer was thus proportional to the lift force acting on the axis.

The driving rod used to excite the pitching modes of oscillation was connected to the root block midway between the positions of the pitching axes. Light alloy angles bridging the brackets bolted to the root block provided an attachment for the springs required for balancing the inertia force.

3.3. *Excitation.*

In each mode the oscillation was maintained by forcing from a swash-plate exciter. The angle of tilt of the swash plate could be varied smoothly to alter the amplitude of oscillation of a plunger projecting from the body of the exciter. Sinusoidal forcing from the plunger was transmitted through a spring and linkage to a driving rod coupled to the wing root. Cross-spring bearings or spring flexures were used throughout to minimise the damping in the apparatus.

3.4. *Frequency Measurement.*

Balance between the spring and inertia forces occurs only at the chosen frequency, and thus to avoid errors in the force measurements this frequency must be accurately maintained.

Frequency was measured at 10 second intervals during the test and corrected by manually adjusting the speed of the exciter motor. An electronic counter[2] measured the frequency to an accuracy of about $\pm 0{\cdot}05\%$ and generally it was maintained to within $\pm 0{\cdot}1\%$ of the chosen value.

3.5. *Force Measurement and Recording.*

Applied forces normal to the mean plane of the wing were measured by force transducers in the driving linkage and at the wing root. (Fig. 2 and Section 2.)

A force transducer is shown in Fig. 6. The ends of two beryllium copper strips were attached to a channel section forming the body of the unit, and these strips were placed in tension by tightening two bolts in a block connected between their centres. Load applied to the connector then caused an increase in tension in one strip and a decrease in the other. Four wire-resistance strain gauges cemented to the strips were connected to form a Wheatstone bridge sensitive to loading in the axial direction.

Output from the galvanometer arm of the Wheatstone bridge was supplied to a pair of brushes bearing at 180° on a two-segment commutator mounted on the shaft of the exciter and rotating at the wing oscillation frequency. Each of the two commutator segments was coupled to an outer slip ring which was connected to the galvanometer. The transducer output was thus reversed in direction after each half cycle of oscillation by the commutator to produce a signal having a mean d.c. level which was measured by the galvanometer. The transducer output could also be switched to a second pair of brushes at 90° to the first pair. Fig. 7 indicates the arrangement of the commutator and Fig. 8 the form of the resultant signals. It may be shown that for a sinusoidal input signal the two galvanometers readings are:

Switched to 1st pair of brushes,

$$\text{response} = -\frac{2}{\pi} S_0 \cos \psi .$$

Switched to 2nd pair of brushes,

$$\text{response} = \frac{2}{\pi} S_0 \sin \psi .$$

From these two readings the amplitudes of the transducer outputs and their phase relationships to the commutator were found. The phase angle between the commutator rotation and the wing displacement depended upon the wing load since the exciting force was applied through a spring. To establish this angle a strain-gauged cantilever strip was connected to the wing and its output also supplied to the commutator and measured by the galvanometer. The cantilever produced a signal in phase with the wing displacement and thus from the two sets of measurements the components of the transducer output in phase and in quadrature with the wing displacement were found.

4. *Test Procedure.*

In each mode the reactions of the inertia forces at the force transducers were reduced by oscillating the wing against earthed springs as described in Section 2. Generally, a precise balance of inertia and stiffness force was not achieved but instead spring stiffnesses and positions were found for which the resulting reactions were well below the level of the aerodynamic forces. These residual forces, in phase with the motion, and the accompanying quadrature forces required to overcome the structural and aerodynamic forces were measured in still air at the chosen frequency and amplitude of oscillation. Measurements were then made at the same frequency and amplitude at wind speeds between 40 ft/sec and 140 ft/sec. Following the wind-on tests a further set of measurements was made in still air. The aerodynamic forces due to the windstream were taken to be the difference between the wind-on and still-air force measurements.

The in-phase forces found in this way correspond to the aerodynamic forces due to displacement alone, since the virtual inertia forces, which are present both with the wind on and in still air, are excluded by the subtraction. Similarly the derived forces in quadrature with the wing motion do not include the still-air aerodynamic damping.

The force transducers were calibrated dynamically by attaching masses to the wing-root assembly and measuring the additional outputs in oscillations at the test frequency and amplitudes.

Static aerodynamic force and moment derivatives were found by disconnecting the main springs and measuring the change of force at each transducer over a range of wing incidence at a fixed wind speed. Corrections were applied for the forces arising from the stiffness of the cross-spring bearings.

5. *Test Programme.*

Measurements were made in the following conditions:

(a) Plain wing.

(b) Wing with transition wire fitted.

(c) Wing with nacelle in central position (*see* Figs. 4 and 5) transition wire fitted to wing and nacelle.

(d) As for (c) with rear of nacelle blocked to prevent flow through.

(e) Wing with nacelle in forward position (*see* Fig. 5) transition wire fitted to wing and nacelle, nacelle open to allow flow through.

(f) Wing with nacelle in rear position (*see* Fig. 5) transition wire fitted to wing and nacelle, nacelle open to allow flow through.

(g) Wing with tip tank (*see* Figs. 4 and 5) transition wire fitted to wing and tank.

(h) Wing with tip tank and rear fin (*see* Figs. 4 and 5) transition wire fitted to wing and tank.

In all cases measurements were made for pitch about both the forward and rear axis positions at a mean angle of incidence of 0°, and generally covered amplitudes of $\pm 2\frac{1}{2}°$ and $\pm 5°$. The frequency of oscillation was 4·98 c/sec throughout, which, for the test wind speeds between 40 ft/sec and 140 ft/sec, gave a range of frequency parameter, based on wing mean chord, from 1·14 to 0·33. The corresponding range of Reynolds number, also based on wing mean chord, was from $0{\cdot}37 \times 10^6$ at frequency parameter 1·14, to $1{\cdot}31 \times 10^6$ at frequency parameter 0·33.

The transition wire on the wing was fixed at 10% of the local chord from the leading edge, and was 0·022 inches in diameter. The transition wire fitted to the nacelle in its forward and central position, and also to the tip tank, was of the same diameter as the wire on the wing and was carried round outside the nacelle or tank as a continuation of the wing transition wire. For the nacelle in the rear position the wire was attached to the outside of the nacelle at a distance of 3·7 inches from its nose.

6. *Presentation of Results.*

The results are given in terms of overall derivatives, and it is shown how these derivatives are related to a set of equivalent constant-strip derivatives* for rigid modes of pitch and translation.

6.1. *Overall Derivatives.*

The total lift and the moment about a reference axis normal to the stream at the root mid-chord, for the modes of oscillation of rigid pitch about the forward and rear axis positions, are expressed in terms of overall derivatives as follows:

(a) *Pitching about the forward axis.*

$$\frac{\text{Total lift}}{\rho V^2 s c_m \alpha} = (l_\theta)_f + i\nu_m (l_{\dot\theta})_f,$$

$$\frac{\text{Total pitching moment}}{\rho V^2 s c_m{}^2 \alpha} = (m_\theta)_f + i\nu_m (m_{\dot\theta})_f.$$

* Equivalent constant-strip derivatives are derivatives which are chosen to be independent of spanwise position but when integrated over the wing in the appropriate mode give the correct generalised forces; the values of the derivatives depend upon the planform, the modes of oscillation, the position of the reference axis, the mean frequency parameter and the Mach number.

(b) *Pitching about the rear axis.*

$$\frac{\text{Total lift}}{\rho V^2 s c_m \alpha} = (l_\theta)_r + i\nu_m (l_{\dot\theta})_r,$$

$$\frac{\text{Total pitching moment}}{\rho V^2 s c_m{}^2 \alpha} = (m_\theta)_r + i\nu_m (m_{\dot\theta})_r.$$

The symbols are defined in the Notation.

Values of $(l_\theta)_f$, $(l_{\dot\theta})_f$ . . . $(m_\theta)_r$ and $(m_{\dot\theta})_r$ are plotted against mean frequency parameter in Figs. 9 to 40.

Values of derivatives for the wing with nacelle and tip tank are based on the area of the wing alone (sc_m) and the mean chord of the wing alone (c_m).

6.2. *Equivalent Constant-Strip Derivatives.*

For a typical chordwise strip the lift and pitching moment about the reference axis may be written:

$$\text{Lift on the strip} = \rho V^2 c\,dy \left\{ (l_\alpha + i\nu l_{\dot\alpha})\alpha + (l_z + i\nu l_{\dot z}) \frac{z}{c} \right\},$$

$$\text{Moment on the strip} = \rho V^2 c^2\,dy \left\{ (m_\alpha + i\nu m_{\dot\alpha})\alpha + (m_z + i\nu m_{\dot z}) \frac{z}{c} \right\}.$$

The symbols are defined in the Notation. Hence, total lift on the half wing

$$= \rho V^2 s c_m \int_0^1 \left\{ \frac{c}{c_m} l_\alpha \alpha + l_z \frac{z}{c_m} \right\} d\eta + i\nu_m \rho V^2 s c_m \int_0^1 \left\{ \frac{c^2}{c_m{}^2} l_{\dot\alpha}\alpha + \frac{c}{c_m} l_{\dot z} \frac{z}{c_m} \right\} d\eta,$$

and total pitching moment about the reference axis normal to the stream at the root mid-chord

$$= \rho V^2 s c_m{}^2 \int_0^1 \left\{ \frac{c^2}{c_m{}^2} m_\alpha \alpha + \frac{c}{c_m} m_z \frac{z}{c_m} \right\} d\eta + i\nu_m \rho V^2 s c_m{}^2 \int_0^1 \left\{ \frac{c^3}{c_m{}^3} m_{\dot\alpha}\alpha + \frac{c^2}{c_m{}^2} m_{\dot z} \frac{z}{c_m} \right\} d\eta.$$

For this particular wing it may be shown that

$$\int_0^1 \frac{c^2}{c_m{}^2}\, d\eta = 1{\cdot}0301; \qquad \int_0^1 \frac{c^3}{c_m{}^3}\, d\eta = 1{\cdot}0904.$$

Thus, in terms of equivalent constant-strip derivatives,

$$\frac{\text{Total lift}}{\rho V^2 s c_m} = l_\alpha \alpha + l_z \frac{z}{c_m} + i\nu_m \left(1{\cdot}0301\, l_{\dot\alpha}\alpha + l_{\dot z} \frac{z}{c_m} \right)$$

$$\frac{\text{Total pitching moment}}{\rho V^2 s c_m{}^2} = 1{\cdot}0301\, m_\alpha \alpha + m_z \frac{z}{c_m} + i\nu_m \left(1{\cdot}0904\, m_{\dot\alpha}\alpha + 1{\cdot}0301\, m_{\dot z} \frac{z}{c_m} \right).$$

(a) *Pitching about the forward axis.* Displacement of the reference axis and pitch are related as follows:

$$\frac{z}{c_m} = 0{\cdot}37063\, \alpha.$$

Hence,

$$\frac{\text{Total lift}}{\rho V^2 s c_m \alpha} = l_\alpha + 0{\cdot}37063\, l_z + i\nu_m (1{\cdot}0301\, l_{\dot\alpha} + 0{\cdot}37063\, l_{\dot z}),$$

$$\frac{\text{Total pitching moment}}{\rho V^2 s c_m{}^2 \alpha} = 1{\cdot}0301\, m_\alpha + 0{\cdot}37063\, m_z + i\nu_m (1{\cdot}0904\, m_{\dot\alpha} + 0{\cdot}3818\, m_{\dot z}).$$

(b) *Pitching about rear axis.* Displacement of the reference axis and pitch are related as follows:

$$\frac{z}{c_m} = -0{\cdot}18881\,\alpha.$$

Hence,

$$\frac{\text{Total lift}}{\rho V^2 s c_m \alpha} = l_\alpha - 0{\cdot}18881\,l_z + iv_m(1{\cdot}0301\,l_{\dot\alpha} - 0{\cdot}18881\,l_{\dot z}),$$

$$\frac{\text{Total moment}}{\rho V^2 s c_m{}^2 \alpha} = 1{\cdot}0301\,m_\alpha - 0{\cdot}18881\,m_z + iv_m(1{\cdot}0904\,m_{\dot\alpha} - 0{\cdot}1945\,m_{\dot z}).$$

Thus, the equivalent constant-strip derivatives are related to the overall derivatives as follows:

$$\begin{aligned}
(l_\theta)_f &= l_\alpha + 0{\cdot}37063\,l_z,\\
(l_{\dot\theta})_f &= 1{\cdot}0301\,l_{\dot\alpha} + 0{\cdot}37063\,l_{\dot z},\\
(m_\theta)_f &= 1{\cdot}0301\,m_\alpha + 0{\cdot}37063\,m_z,\\
(m_{\dot\theta})_f &= 1{\cdot}0904\,m_{\dot\alpha} + 0{\cdot}3818\,m_{\dot z},\\
(l_\theta)_r &= l_\alpha - 0{\cdot}18881\,l_z,\\
(l_{\dot\theta})_r &= 1{\cdot}0301\,l_{\dot\alpha} - 0{\cdot}18881\,l_{\dot z},\\
(m_\theta)_r &= 1{\cdot}0301\,m_\alpha - 0{\cdot}18881\,m_z,\\
(m_{\dot\theta})_r &= 1{\cdot}0904\,m_{\dot\alpha} - 0{\cdot}1945\,m_{\dot z}.
\end{aligned}$$

By solving these equations values for the individual equivalent constant-strip derivatives, $l_\alpha \ldots m_{\dot z}$, may be found from the values of the overall derivatives.

7. *Discussion of Results and Comparison with Theory.*

7.1. *Corrections for Wind-Tunnel Interference.*

Two sources of error in the measured coefficients due to wind-tunnel interference have been considered: the first arises from the restraint imposed on the windstream by the walls of the working section, and the second from the possible disturbance to the vortex trail caused by the fan (*see* Fig. 1).

Theoretical corrections for the presence of the walls have been calculated by W. P. Jones[3] and by Acum and Garner[4] for oscillating wings in the centre of rectangular- and circular-section closed wind tunnels, respectively. Their results show that the correction to the stiffness derivatives is a maximum at low frequency parameter, and that the correction to the damping derivatives is negligible. Estimates of the steady-state corrections for the test boundary conditions[1] indicate that the measured stiffness derivatives at low frequency parameter are approximately 2% larger than the free-stream values. Corrections of this order are not considered significant and they have therefore been neglected.

Jordan[5] has investigated the effect of curtailing the vortex trail in two-dimensional incompressible flow. Under these conditions, and making the extreme assumption that the wake is terminated at the fan, the oscillatory forces measured on a wing in the test position, and at the test frequency parameters, would be in error by a maximum of 3%. The magnitude of these effects will be altered by the finite span of the test wing, and in view of this uncertainty and the small size of the predicted errors, these corrections also have not been applied.

7.2. *Corrections for Rig Deformation.*

The wing and support frame is subject to deformation under the aerodynamic and inertia loading, resulting in a change in the mode of oscillation with the wind-on from the still-air condition which alters the balance between the inertia and spring forces. Corrections for this effect, and the related change in aerodynamic force, were considered in detail following earlier tests with a larger and heavier model[6]. Analysis showed then that the errors were negligible, and since it is considered that the corresponding corrections for the present model are smaller they have not been calculated.

7.3. *Effects of Amplitude of Oscillation and Transition.*

Under steady conditions the flow over the test wing would be expected to change with incidence in the following way[7]:

(a) At small angles the flow is attached over practically the full wing surface and the lift force and pitching moment vary linearly with incidence.

(b) As the incidence is increased the flow separates from the sharp leading edge and reattaches behind to form a separation bubble.

(c) In addition to separation at the leading edge the flow will also separate at the blunt wing tips at low angles of incidence.

The flow over the test wing was not investigated and thus the sequence of changes (b) and (c) above is not known but both effects should appear in the test range of incidence from $-5°$ to $+5°$. Each effect modifies the rate of change of lift with incidence. Generally leading-edge separation reduces the slope of the lift curve very slightly, and tip separation increases it. For a rectangular wing of aspect ratio 1 Küchemann[7] indicates that the influence of the tip vortex increases the lift at 5° from the zero lift incidence by between 5 and 10%, and that the lift increment acts behind the centre of pressure for attached flow.

In oscillatory motion the flow should be of a generally similar character to that described above, although the angles for separation and reattachment may be altered. The non-linear relationship between aerodynamic force and incidence will affect both the stiffness and the damping derivatives. In the present tests measurements were made at amplitudes of oscillation of $\pm 2\frac{1}{2}°$ and $\pm 5°$, about a mean incidence of 0°, and the results provide an indication of the overall effects of the changes in flow conditions. For the wing alone increase in amplitude increased the stiffness lift and moment derivatives; the increase in lift force of approximately 10% being proportionally greater than the increase in moment. These results are consistent with the effect of the tip vortex in steady flow. Accompanying the increase in stiffness force the measurements show a decrease in the damping force derivatives, and certain reductions in the damping moment derivatives; for pitch about the rear axis the damping moment derivatives decreased by an amount which was approximately independent of frequency parameter, whereas for pitch about the forward axis a proportionally larger reduction occurred at the lowest test frequency parameters with the change becoming small at frequency parameter 0·6.

With nacelle and tip tank fitted the effects of increasing amplitude were generally similar in trend but smaller in magnitude than for the wing alone. In steady flow increasing the aspect ratio reduces the lift increment arising from the tip vortex, and thus fitting the nacelle and tip tank, which increases the effective aspect ratio of the wing assembly, could be expected to reduce the change in the values of the derivatives with amplitude.

Comparison of the results for the plain wing (Figs. 9 to 12) with those for the wing with transition wire (Figs. 13 to 16) indicates that adding the wire produced only small changes in the values of the derivatives.

7.4. *Derivatives for the Wing Alone.*

Experimental results for the plain wing are given in Figs. 9 to 12, and results for the wing with transition wire fitted are given in Figs. 13 to 16 together with values calculated using lifting-surface theory and a semi-empirical method. The lifting-surface-theory derivatives were calculated using the R.A.E. Deuce digital-computer programme of Richardson's method. The semi-empirical derivatives were found in the way described in the A.G.A.R.D. Manual of Aeroelasticity[8]; this is an extension of the procedure suggested by Minhinnick[9], and its application to the present case is indicated in Appendix I.

With the exception of $(m_{\dot{\theta}})_f$ at 5° amplitude, the measured derivatives are practically independent of frequency parameter over the test range. The derivative $(m_{\dot{\theta}})_f$ also appears to be independent of frequency parameter at the lower test amplitude and its value agrees well with the values for 5° amplitude at frequency parameters greater than 0·6.

The theoretical derivatives are also practically independent of frequency parameter. The semi-empirical values are by definition independent of frequency parameter for the test-wing aspect ratio.

Comparison of the measured and calculated results indicates that there is generally good agreement between the three sets of lift derivatives but that there are some discrepancies between the corresponding values of the moment derivatives. In general the values predicted by the semi-empirical method agree quite closely with those found using lifting-surface theory, but where there are significant differences between the calculated and measured results the lifting-surface values are more accurate. It should be noted that the centre of action of the damping force is close to the reference axis at the mid-chord, and thus the chosen method of presentation gives emphasis to the differences between the sets of damping moment derivatives. For pitch about the forward axis, for example, the relatively large discrepancies arise because the resultant damping force acts $2\frac{1}{2}\%$ of the mean chord ahead of the position predicted by lifting-surface theory, and 4% of the mean chord ahead of the position predicted by the semi-empirical method.

7.5. *Derivatives for the Wing with Nacelle.*

Measured derivatives for the wing with the nacelle in the forward, central and rear positions for the condition in which there was flow through the nacelle are plotted against frequency parameter in Figs. 17 to 20, 21 to 24, and 25 to 28, respectively. Results for the nacelle with its rear blocked to prevent flow through are given in Figs. 29 to 32 for the central position. Values of derivatives calculated using a semi-empirical method (*see* Appendix II) for the wing with nacelle in the central position are included in Figs. 21 to 24.

Comparison of the sets of results for the nacelle with flow through shows that:

$(l_{\dot{\theta}})_f$ is practically independent of the nacelle position, but the values under oscillatory conditions are slightly smaller than the static value

$(l_{\dot{\theta}})_f$ increases as the nacelle moves back, and for the central and rear positions decreases slightly with increasing frequency parameter

$(m_\theta)_f$ decreases as the nacelle moves back, and in each position decreases with increasing frequency parameter

$(m_{\dot\theta})_f$ decreases as the nacelle moves back, but is practically independent of frequency parameter

$(l_\theta)_r$ is practically independent of the nacelle position, but decreases with increasing frequency parameter

$(l_{\dot\theta})_r$ increases as the nacelle moves from the forward to the central position, but there is no further change with movement to the rear position. In each position there is a small increase in value with increasing frequency parameter

$(m_\theta)_r$ decreases as the nacelle moves back and in each position decreases slightly with increasing frequency parameter

$(-m_{\dot\theta})_r$ is approximately independent of position and frequency parameter for the central and rear positions. At the forward position the value decreases slightly with increasing frequency parameter but at frequency parameters between 0·3 and 0·6 it agrees fairly well with the values for the central and rear positions.

Comparing these results with the results for the wing alone (and remembering that both sets were made non-dimensional by dividing by the plain-wing area and mean chord) it is apparent that adding the nacelle increases the stiffness lift force by about 50%.

Moving the nacelle from the forward to central position brings the centre of action of the stiffness lift back by approximately 3% of the mean chord of the plain wing, and practically the same displacement takes place when the nacelle is moved from the central to the rear position. The amount of movement of the centre of action is almost the same for both pitching axes although the absolute positions do not coincide. The stiffness lift forces of the wing alone act at points between the corresponding centres of action for the wing with nacelle forward and central.

The derivative $(l_{\dot\theta})_f$ for the wing with nacelle is also approximately 50% larger than the value for the wing alone, and its centre of action moves back approximately 2% of the mean chord for each change of nacelle position from the front to the rear. For the wing alone the damping lift force for pitch about the forward axis acts at a point just behind the corresponding position with the wing with nacelle central. The derivative $(l_{\dot\theta})_r$ depends upon frequency parameter and nacelle position and the value for the wing alone at low frequency parameter lies between the values for the nacelle forward and central. The centre of action of the corresponding damping force for the wing alone is farther forward than in any of the nacelle configurations.

The effect of preventing flow through the nacelle in the central position may be found from Figs. 21 to 24 and Figs. 29 to 32. Comparison shows that blocking the nacelle generally produced only small changes in the values of the derivatives. An exception to this is the damping lift force for oscillations about the forward axis which increased slightly and moved forward approximately 2% of the mean chord at the lower test frequency parameters.

The derivatives calculated for the wing with nacelle in the central position, and shown on Figs. 21 to 24, are in reasonable agreement with the measured values. One of the assumptions made in the semi-empirical method of calculation is that for wings of aspect ratio less than 3 the derivatives are independent of frequency parameter. This holds true in general for plain-wing surfaces. Although the effective aspect ratio of the wing with nacelle is within this range, the

measured derivatives $(l_\theta)_f$, $(l_\theta)_r$ and $(m_\theta)_f$ decrease as the frequency parameter is increased, and this gives rise to discrepancies between the measured results and the corresponding calculated stiffness derivatives, which are made equal to the calculated static values. The errors in $(l_\theta)_f$ and $(l_\theta)_r$ are approximately 10%, and the error in $(m_\theta)_f$ is rather larger. The method of estimating the damping derivatives is more complicated than for the stiffness derivatives, but the resulting values of $(l_{\dot\theta})_f$ and $(l_{\dot\theta})_r$ are also accurate to within about 10%. The predicted centre of action of the damping force is about 2% of the mean chord behind the measured position for pitching about the forward axis, and 8% behind for pitching about the rear axis.

If it is necessary to estimate the aerodynamic forces with an accuracy better than this then the semi-empirical method described clearly needs some modification. It should be noted, however, that in most practical flutter calculations, derivatives are required for modes of deformation rather than for the rigid modes used in the measurements. Thus an arbitrary change of the calculated values to give agreement for the test modes will not necessarily prove satisfactory for general application. The semi-empirical method does, of course, take account of the mode of oscillation, in the same way as the semi-empirical method for plain surfaces (*see* Appendix I).

7.6. *Derivatives for the Wing with Tip Tank.*

Results for the wing with tip tank fitted are plotted against frequency parameter in Figs. 33 to 36, and corresponding results with the fin added to the rear of the tank are given in Figs. 37 to 40.

The derivatives for the wing with tank are all larger than the corresponding values for the wing alone, but slightly smaller than the values for the wing with nacelle.

Adding the fin to the rear of the tank increases the stiffness lift and reduces the stiffness moment at both axis positions. These results are consistent with the development of lift on the fin proportional to the incidence. For pitching about the forward axis the damping lift generally increases and the damping moment about the reference axis decreases; for pitching about the rear axis both the damping lift and moment decrease slightly. If the fin was treated as an isolated surface oscillating in pitch about forward axes at the same relative positions as in the test, then the damping lift would increase and the moment decrease at both axis positions. Comparing the results of a simple calculation of this sort with the test results shows that the measured increases of the stiffness lift and moment are three to four times larger than the predicted changes; the measured changes of damping moment are about the same magnitude as the estimated changes, and the measured increase of damping lift is smaller than the calculated increase at the forward axis, and of opposite sign at the rear axis. The discrepancies between these sets of results clearly arise from the interference effects of the wing and tank, and it is interesting to note that measurements by Clevenson and Leadbetter[10] on a wing with a tip tank oscillating about an axis at the mid-chord also indicated that the damping lift decreased when the tank was fitted with a rear fin. Their measurements showed in addition that the direct damping moment decreased. This did not occur in the present tests but will, no doubt, depend upon the particular tank and fin configuration.

A conclusion from these tests is that although the addition of a rear fin to a tip body may produce very approximately the expected change in the stiffness forces, the corresponding change in the damping forces cannot be predicted with confidence. Thus a fin may reduce the aerodynamic damping in a torsion mode instead of increasing it, and this effect should be borne in mind in making flutter calculations.

8. *Conclusions.*

Lift and pitching-moment derivatives have been measured on the following wing and wing-body combinations oscillating in pitch about two spanwise axes at low subsonic wind speeds:

(i) tapered wing of aspect ratio 1·3, mid-chord line unswept, with a sharp leading edge,

(ii) above wing fitted with a nacelle in three chordwise positions at the tip,

(iii) wing at (i) fitted with a tip body representing a tank or store, and tested with and without a fin at the rear of the body.

The measurements were made for oscillations about a mean angle of incidence of 0° at amplitudes of $\pm 2\frac{1}{2}°$ and $\pm 5°$, and covered a range of frequency parameter from 0·33 to 1·14 at Reynolds numbers between $0{\cdot}37 \times 10^6$ and $1{\cdot}31 \times 10^6$.

The results show that:

(a) Increasing amplitude from $2\frac{1}{2}°$ to 5° generally altered the values of the derivatives. The maximum change occurred for the wing alone and was of the order of 10%.

(b) Derivatives calculated for the wing alone using lifting-surface theory, which strictly applies for oscillations of infinitesimal amplitude, are nevertheless in good agreement with the measured values.

(c) Derivatives calculated for the wing alone using a semi-empirical method are in reasonable agreement with the measured values.

(d) The addition of a nacelle to the wing tip significantly increased the oscillatory lift forces and moments, and the magnitude of the increases depended upon the nacelle position; generally the variation of the pitching-moment derivatives with nacelle chordwise position was greater than that of the lift derivatives.

(e) Derivatives calculated for the wing with nacelle in the central position (using a semi-empirical method which makes an allowance for the aerodynamic interference effects) are in reasonable agreement with the measured values.

(f) The addition of a streamlined body representing a tank or store at the wing tip significantly increased the magnitude of the oscillatory lift forces and moments, although in the test case the increases were not so great as those produced by the nacelle.

(g) The addition of a fin at the rear of the tank changed slightly the oscillatory forces and moments; the changes could not be predicted satisfactorily by treating the fin as an isolated surface.

NOTATION

c		Local wing chord
c_m		Mean wing chord $\left(= \frac{\text{wing area}}{\text{span}}\right)$, 1·487 ft
s		Wing semi-span, 0·949 ft
y		Distance of chordwise strip from root
dy		Width of chordwise strip
z		Displacement in normal translation of reference axis through wing-root mid-chord, normal to windstream, measured positive downwards
S_0		Amplitude of transducer output
V		Wind velocity
α		Angle of pitch, positive nose up
η	$=$	y/s
ν		Local frequency parameter $\left(= \frac{\omega c}{V}\right)$
ν_m		Mean frequency parameter $\left(= \frac{\omega c_m}{V}\right)$
ρ		Air density
ψ		Phase angle between commutator rotation and transducer output
ω		Circular frequency of oscillation
l_α, l_z		Non-dimensional, stiffness lift derivatives for motion in pitch and normal translation, respectively
$l_{\dot\alpha}$, $l_{\dot z}$		Non-dimensional, damping lift derivatives for motion in pitch and normal translation, respectively. Lift measured positive upwards
m_α, m_z		Non-dimensional, stiffness pitching-moment derivatives for motion in pitch and normal translation, respectively
$m_{\dot\alpha}$, $m_{\dot z}$		Non-dimensional, damping pitching-moment derivatives for motion in pitch and normal translation, respectively. Moment measured about reference axis through wing-root mid-chord, positive nose up
$(l_\theta)_f$, $(l_\theta)_r$		Non-dimensional, overall stiffness lift derivatives for pitching motion about forward and rear axis positions, respectively
$(l_{\dot\theta})_f$, $(l_{\dot\theta})_r$		Non-dimensional, overall damping lift derivatives for pitching motion about forward and rear axis positions, respectively. Lift measured positive upwards
$(m_\theta)_f$, $(m_\theta)_r$		Non-dimensional, overall stiffness pitching-moment derivatives for pitching motion about forward and rear axis positions, respectively
$(m_{\dot\theta})_f$, $(m_{\dot\theta})_r$		Non-dimensional, overall damping pitching-moment derivatives for pitching motion about forward and rear axis positions, respectively. Moment measured about reference axis through wing-root mid-chord, positive nose up

REFERENCES

No.	Author(s)	Title, etc.
1	P. R. Guyett and J. K. Curran ..	Aerodynamic derivative measurements on a rectangular wing of aspect ratio 3·3. A.R.C. R. & M. 3171. March, 1958.
2	W. D. T. Hicks..	An electronic instrument for the accurate measurement of the frequency of structural oscillations. A.R.C. 17 920. January, 1955.
3	W. P. Jones	Wind tunnel interference effect on the values of experimentally determined derivative coefficients for oscillating aerofoils. A.R.C. R. & M. 1912. August, 1943.
4	W. E. A. Acum and H. C. Garner ..	Approximate wall corrections for an oscillating swept wing in a wind tunnel of closed circular section. A.R.C. C.P. 184. January, 1954.
5	P. F. Jordan	The harmonically oscillating wing with finite vortex trail. A.R.C. R. & M. 3038. July, 1953.
6	P. R. Guyett and J. K. Curran ..	Aerodynamic derivative measurements on a wing with a horn-balanced control surface. A.R.C. R. & M. 3307. March, 1961.
7	D. Küchemann	A simple method of calculating the span and chordwise loading on straight and swept wings of any given aspect ratio at subsonic speeds. A.R.C. R. & M. 2935. August, 1952.
8	P. R. Guyett	Empirical values of derivatives. AGARD *Manual of Aero-elasticity*, Part II, Chapter 11. 1961.
9	I. T. Minhinnick	Aerodynamic derivatives. Paper 4 of 'A symposium on the flutter problem in aircraft design'. H. Templeton and G. R. Brooke, editors. Unpublished M.o.A. Report.
10	S. A. Clevenson and S. A. Leadbetter	Some measurements of aerodynamic forces and moments at subsonic speeds on a wing-tank configuration oscillating in pitch about the wing midchord. N.A.C.A. Tech Note 3822. December, 1956.
11	H. R. Lawrence and E. H. Gerber ..	The aerodynamic forces on low aspect ratio wings oscillating in an incompressible flow. *J. Ae. Sci.*, Vol. 19, No. 11. November, 1952.
12	D. E. Hartley	Theoretical load distributions on wings with cylindrical bodies at the tips. A.R.C. C.P. 147. June, 1952.
13	J. De Young and C. W. Harper ..	Theoretical symmetric span loading at subsonic speeds for wings having arbitrary planform. N.A.C.A. Report 921. 1948.

APPENDIX I

Semi-Empirical Derivatives for the Wing Alone (Figs. 13 to 16)

The semi-empirical derivatives were found using the method described in the AGARD Flutter Manual[8]. This method is an extension of the procedure suggested by Minhinnick[9].

Derivatives for a mode of rigid translation were calculated as follows:

(a) The values of the true strip derivatives† $l_{\dot{z}}$ were assumed equal to the corresponding values of l_α for a mode of rigid pitch in steady flow. The required local values of l_α were found using Multhopp's method[7].

(b) Values for $m_{\dot{z}}$ were found from the values of $l_{\dot{z}}$ and the local chordwise position of the aerodynamic centre determined from Ref. 7.

(c) $l_{\dot{z}}$ and $m_{\dot{z}}$ were considered to be independent of frequency parameter.

(d) It was assumed that $l_z = m_z = 0$.

Derivatives for a mode of rigid pitch about the root mid-chord were calculated as follows:

(e) Local values of the true strip derivatives l_α were found from the distribution of lift for a mode of rigid pitch in steady flow as at (a) above.

(f) The true strip derivatives m_α were found from the appropriate values of l_α and the local chordwise position of the aerodynamic centre {*see* (b) above}.

(g) The damping lift was found by considering the motion in pitch about the root mid-chord to be composed of a mode of translation without pitch (mode 1), in which the displacement was equal to the displacement of the leading edge in the original pitch mode, together with a rigid surface motion in pitch without translation of the wing leading edge (mode 2). Values of the local strip derivatives $l_{\dot{z}}$ for the translation mode 1 above were assumed to be equal to the local values of l_α in steady flow for a mode of twist in which the distribution of incidence was equal to the local displacement in translation. Values of the derivatives for pure pitch, mode 2, were found from the local steady-flow values of l_α for a mode of pure pitch, multiplied by the ratio $l_{\dot{\alpha}}^*/l_\alpha^*$, where: $l_{\dot{\alpha}}^*$ is the equivalent constant-strip derivative for damping lift due to pitching motion about the leading edge of a rectangular wing, and l_α^* is the corresponding equivalent constant-strip derivative for stiffness lift due to pitching motion about the leading edge of a rectangular wing. The values of $l_{\dot{\alpha}}^*$ and l_α^* were taken from graphs given in Ref. 8, which were based on results calculated by Lawrence and Gerber[11], and refer to a rectangular wing of the same aspect ratio as the test wing. For aspect ratios lower than about three the values of the derivatives are independent of frequency parameter. The total damping lift for the mode of pitch about the root mid-chord was found by adding together the above values for the translation mode 1 and the pitch mode 2.

(h) The damping moment due to pitch was determined by estimating the local chordwise points of action of the damping lift forces due to translation and pitch given above at (g). The damping lift force due to translation in mode 1 was assumed to act at the local chordwise position of the aerodynamic centre. {See (b) above.} The damping lift force due to pitch in mode 2 was assumed to act at a fraction of the local chord from the leading edge given by $m_{\dot{\alpha}}^*/l_{\dot{\alpha}}^*$, where $m_{\dot{\alpha}}^*$ and $l_{\dot{\alpha}}^*$ are equivalent constant-strip derivatives for a rectangular wing with the reference axis at the

† Derivatives which vary with spanwise position and give the correct local loads.

leading edge, found from Ref. 8 or 11 for the test-wing aspect ratio. The total damping moment for the mode of pitch about the root mid-chord was found by adding together the moments for the translation mode 1 and pitch mode 2.

Although this procedure may appear complicated it can be used to give what are believed to be reliable answers for modes of structural deformation. For modes of this type the straightforward Minhinnick approach is often inaccurate.

APPENDIX II

Semi-Empirical Derivatives for Wing with Nacelle in Central Position (Figs. 21 to 24)

These values were also found using the method described in the AGARD Flutter Manual[8].

The method requires a knowledge of the spanwise distribution of steady lift force over the wing and nacelle due to uniform incidence. For the test wing this was calculated from the theoretical results in Ref. 12. The procedure was then as follows:

(i) From the total lift force on the wing surface alone the effective wing aspect ratio was found from Ref. 13.

(ii) The steady loads on the isolated wing alone for uniform pitch, found in Appendix I above, were subtracted from the calculated total loads on the wing in the presence of the nacelle. The remainder represented the interference load due to the nacelle.

(iii) The steady load due to incidence on the nacelle, treated as an isolated unit, was found using slender-body theory. This force was subtracted from the calculated lift on the nacelle in the presence of the wing. The remainder represents the interference load on the nacelle due to the wing.

(iv) Derivatives for wing and nacelle motion were then calculated using the approach described in Appendix I above, with the following additions:

(v) The load on the wing surface was treated in two parts: one part was the loading on the original plain wing found in the way described in Appendix I {but *see* notes (vi) and (vii) below}, the second part was the interference loading due to the nacelle {(ii) above}. This interference loading and the derived stiffness and damping forces and moments were assumed to depend solely upon the motion of the nacelle, referred to an axis at the wing-tip leading edge.

(vi) All the lift on the wing surface arising from the l_α and $l_{\dot{z}}$ strip derivatives was assumed to act at the local chordwise centre of pressure for the effective wing aspect ratio {*see* (i) above}.

(vii) Required values of the equivalent constant-strip derivatives $l_\alpha{}^*$, $l_{\dot{\alpha}}{}^*$, $m_{\dot{\alpha}}{}^*$ {Appendix I(g) and (h)} were also found for the effective aspect ratio at (i) above.

(viii) The load on the nacelle was also treated in two parts. One set of forces was found directly from the motion of the nacelle using slender-body theory. The second set represented the load due to the presence of the wing and was also related to the motion of the nacelle. The lift forces of the second set of loads were found in the same way as the lift forces on the plain wing (*see* Appendix I) but using the effective wing aspect ratio at (i) above, and (vii). These forces were assumed to act on the nacelle at a point adjacent to the chordwise centre of action of the corresponding loads on the wing at the tip.

TABLES

All the tests were made with the wing at 0° mean incidence.

The results given are not corrected for wind-tunnel interference.

The test Reynolds number varied between $0{\cdot}4 \times 10^6$ at frequency parameter $1{\cdot}1$, and $1{\cdot}3 \times 10^6$ at frequency parameter $0{\cdot}3$. (Reynolds number and frequency parameter both based on wing mean chord.)

TABLE 1

Results for Plain Wing

Frequency parameter ν_m	Forward axis				Rear axis			
	$(l_\theta)_f$	$(l_{\dot\theta})_f$	$(m_\theta)_f$	$(m_{\dot\theta})_f$	$(l_\theta)_r$	$(l_{\dot\theta})_r$	$(m_\theta)_r$	$(m_{\dot\theta})_r$
Amplitude $\pm 5°$								
0·331	0·949 0·964	1·031 1·071	0·269 0·274	0·027 0·029				
0·385	0·953 0·957	1·041 1·056	0·268 0·267	0·028 0·036	1·003 1·010	0·536 0·555	0·292 0·297	−0·115 −0·119
0·462	0·947 0·965	1·016 1·053	0·267 0·272	0·028 0·050	0·965 0·994	0·524 0·588	0·288 0·283	−0·118 −0·122
0·576	0·982 0·981	0·963 1·034	0·274 0·271	0·030 0·047	0·976 0·995	0·540 0·594	0·291 0·299	−0·122 −0·117
0·764	0·957 0·975	1·031 1·034	0·276 0·267	0·046 0·052	1·043 0·987	0·540 0·546	0·285 0·291	−0·124 −0·122
1·137	0·953 0·949	0·959 0·970	0·277 0·267	0·041 0·044				
Amplitude $\pm 2·5°$								
0·331	0·893 0·877	1·152 1·137	0·268 0·262	0·068 0·061				
0·385	0·869 0·880	1·132 1·124	0·259 0·260	0·048 0·056				
0·462	0·866 0·910	1·228 1·107	0·256 0·261	0·082 0·053				
0·576	0·846 0·893	1·065 1·143	0·247 0·261	0·045 0·058				

TABLE 2

Results for Wing with Transition Wire

Frequency parameter ν_m	Forward axis				Rear axis			
	$(l_\theta)_f$	$(l_{\dot\theta})_f$	$(m_\theta)_f$	$(m_{\dot\theta})_f$	$(l_\theta)_r$	$(l_{\dot\theta})_r$	$(m_\theta)_r$	$(m_{\dot\theta})_r$
Amplitude $\pm 5°$								
0·331	0·955 0·946	0·947 0·983	0·269 0·268	0·017 0·022				
0·385	0·975 0·946	0·999 0·991	0·273 0·265	0·035 0·035	0·956 0·944	0·476 0·439	0·288 0·299	−0·133 −0·125
0·462	0·955 0·950	1·025 1·020	0·265 0·265	0·050 0·046	0·893 0·926	0·477 0·513	0·298 0·290	−0·132 −0·124
0·576	0·928 0·916	1·015 0·969	0·258 0·260	0·050 0·043	0·889 0·910	0·563 0·482	0·288 0·287	−0·128 −0·136
0·764	0·911 1·007	0·949 0·955	0·251 0·261	0·047 0·045	0·858 0·899	0·536 0·567	0·293 0·301	−0·126 −0·121
1·137	0·947 1·017	0·938 0·906	0·243 0·254	0·056 0·048	0·857 0·857	0·571 0·567	0·273 0·308	−0·118 −0·110
Amplitude $\pm 2·5°$								
0·331	0·892 0·891	1·068 1·031	0·258 0·258	0·054 0·045				
0·385	0·895 0·878	1·113 1·061	0·261 0·254	0·054 0·049	0·844 0·830	0·628 0·581	0·285 0·274	−0·124 −0·136
0·462	0·917 0·888	1·059 0·996	0·261 0·251	0·057 0·050	0·849 0·852	0·693 0·710	0·286 0·275	−0·110 −0·131
0·576	0·917 0·905	1·025 1·079	0·257 0·250	0·043 0·057	0·824 0·868	0·601 0·648	0·273 0·266	−0·128 −0·126

TABLE 3

Results for Wing with Nacelle in Forward Position

Frequency parameter ν_m	Forward axis				Rear axis			
	$(l_\theta)_f$	$(l_{\dot\theta})_f$	$(m_\theta)_f$	$(m_{\dot\theta})_f$	$(l_\theta)_r$	$(l_{\dot\theta})_r$	$(m_\theta)_r$	$(m_{\dot\theta})_r$
				Amplitude $\pm 5°$				
0·331	1·505 1·485	1·331 1·319	0·438 0·432	0·074 0·069	1·407 1·466	0·445 0·544	0·451 0·464	−0·180 −0·166
0·385	1·477 1·439	1·326 1·316	0·429 0·419	0·089 0·070	1·400 1·501	0·548 0·584	0·461 0·449	−0·166 −0·184
0·462	1·510 1·465	1·246 1·282	0·429 0·431	0·067 0·067	1·453 1·365	0·531 0·494	0·464 0·453	−0·157 −0·181
0·576	1·502 1·501	1·340 1·281	0·434 0·437	0·122 0·076	1·460 1·426	0·601 0·552	0·466 0·467	−0·156 −0·164
0·764	1·531 1·498	1·336 1·298	0·440 0·433	0·114 0·090	1·337 1·393	0·551 0·576	0·431 0·465	−0·150 −0·154
1·137	1·433	1·276	0·377	0·104	1·442 1·450	0·630 0·565	0·404 0·401	−0·111 −0·140
				Amplitude $\pm 2·5°$				
0·331	1·456 1·457	1·349 1·349	0·413 0·416	0·091 0·094	1·477 1·434	0·501 0·508	0·456 0·461	−0·178 −0·190
0·385	1·407 1·458	1·394 1·420	0·395 0·407	0·110 0·122	1·452 1·434	0·475 0·485	0·438 0·435	−0·174 −0·185
0·462	1·480 1·473	1·408 1·332	0·426 0·408	0·108 0·093	1·450 1·437	0·537 0·451	0·442 0·445	−0·169 −0·192
0·576	1·426 1·480	1·300 1·333	0·404 0·414	0·094 0·096	1·404 1·531	0·594 0·518	0·443 0·417	−0·161 −0·177

TABLE 4

Results for Wing with Nacelle in Central Position

Frequency parameter ν_m	Forward axis				Rear axis			
	$(l_\theta)_f$	$(l_{\dot\theta})_f$	$(m_\theta)_f$	$(m_{\dot\theta})_f$	$(l_\theta)_r$	$(l_{\dot\theta})_r$	$(m_\theta)_r$	$(m_{\dot\theta})_r$
				Amplitude $\pm 5°$				
0·331	1·514 1·544	1·508 1·485	0·406 0·406	0·065 0·065	1·497 1·535	0·613 0·611	0·436 0·441	−0·181 −0·168
0·385	1·533 1·507	1·505 1·495	0·401 0·395	0·072 0·086	1·509 1·536	0·676 0·660	0·437 0·442	−0·185 −0·163
0·462	1·502 1·529	1·449 1·458	0·391 0·400	0·071 0·079	1·434 1·527	0·676 0·712	0·445 0·439	−0·164 −0·157
0·576	1·491 1·482	1·420 1·413	0·392 0·383	0·067 0·078	1·517 1·468	0·612 0·622	0·421 0·428	−0·181 −0·173
0·764	1·490 1·514	1·416 1·378	0·389 0·384	0·081 0·072	1·407 1·457	0·678 0·688	0·424 0·413	−0·170 −0·177
1·137	1·500 1·476	1·402 1·338	0·375 0·360	0·094 0·081	1·430 1·531	0·697 0·713	0·403 0·401	−0·155 −0·175
				Amplitude $\pm 2·5°$				
0·331	1·510 1·509	1·500 1·560	0·384 0·388	0·072 0·100	1·546 1·552	0·647 0·623	0·435 0·438	−0·187 −0·200
0·385	1·489 1·521	1·519 1·557	0·382 0·385	0·106 0·089	1·516 1·559	0·612 0·644	0·425 0·435	−0·186 −0·170
0·462	1·511 1·502	1·532 1·534	0·382 0·389	0·086 0·088	1·513 1·491	0·626 0·721	0·424 0·434	−0·165 −0·140
0·576	1·547 1·537	1·557 1·454	0·385 0·388	0·099 0·074	1·403 1·424	0·648 0·653	0·416 0·417	−0·192 −0·169

TABLE 5

Results for Wing with Nacelle in Rear Position

Frequency parameter ν_m	Forward axis				Rear axis			
	$(l_\theta)_f$	$(l_{\dot\theta})_f$	$(m_\theta)_f$	$(m_{\dot\theta})_f$	$(l_\theta)_r$	$(l_{\dot\theta})_r$	$(m_\theta)_r$	$(m_{\dot\theta})_r$
Amplitude $\pm 5°$								
0·331	1·480 1·529	1·537 1·618	0·344 0·360	0·032 0·054	1·468 1·479	0·590 0·680	0·379 0·386	−0·202 −0·177
0·385	1·560 1·511	1·664 1·586	0·368 0·358	0·054 0·054	1·507 1·509	0·668 0·619	0·378 0·396	−0·184 −0·191
0·462	1·533 1·538	1·512 1·584	0·354 0·358	0·045 0·060	1·457 1·470	0·665 0·634	0·379 0·374	−0·172 −0·171
0·576	1·521 1·489	1·522 1·491	0·361 0·328	0·055 0·054	1·460 1·451	0·682 0·682	0·368 0·370	−0·165 −0·169
0·764	1·549 1·549	1·435 1·435	0·359 0·338	0·043 0·051	1·377 1·325	0·710 0·690	0·373 0·348	−0·165 −0·171
1·137	1·578 1·423	1·378 1·441	0·344 0·340	0·061 0·059	1·233 1·408	0·755 0·686	0·356 0·314	−0·199 −0·158
Amplitude $\pm 2·5°$								
0·331	1·507 1·527	1·703 1·676	0·346 0·347	0·071 0·062	1·509 1·526	0·648 0·614	0·363 0·371	−0·183 −0·171
0·385	1·528 1·539	1·715 1·689	0·344 0·341	0·064 0·070	1·486 1·513	0·572 0·710	0·364 0·365	−0·171 −0·167
0·462	1·524 1·522	1·527 1·560	0·335 0·342	0·044 0·055	1·489 1·457	0·636 0·585	0·361 0·363	−0·182 −0·169
0·576	1·490 1·528	1·604 1·546	0·323 0·337	0·060 0·060	1·427 1·417	0·586 0·593	0·353 0·356	−0·189 −0·174

TABLE 6

Results for Wing with Nacelle in Central Position with Rear of Nacelle Blocked

Frequency parameter ν_m	Forward axis				Rear axis			
	$(l_\theta)_f$	$(l_{\dot\theta})_f$	$(m_\theta)_f$	$(m_{\dot\theta})_f$	$(l_\theta)_r$	$(l_{\dot\theta})_r$	$(m_\theta)_r$	$(m_{\dot\theta})_r$
				Amplitude $\pm 5°$				
0·331	1·484 1·500	1·518 1·612	0·392 0·392	0·102 0·117	1·459 1·445	0·652 0·634	0·434 0·439	−0·166 −0·167
0·385	1·539 1·500	1·547 1·498	0·383 0·400	0·101 0·096	1·491 1·473	0·642 0·597	0·432 0·432	−0·156 −0·159
0·462	1·478 1·480	1·503 1·445	0·392 0·383	0·089 0·092	1·471 1·484	0·635 0·609	0·431 0·431	−0·165 −0·182
0·576	1·516 1·489	1·432 1·433	0·394 0·394	0·092 0·096	1·550 1·526	0·618 0·662	0·429 0·433	−0·171 −0·171
0·764	1·530 1·510	1·434 1·414	0·399 0·401	0·098 0·094	1·471 1·464	0·704 0·687	0·432 0·440	−0·178 −0·163
1·137	1·516 1·476	1·384 1·320	0·391 0·389	0·099 0·076	1·572 1·572	0·786 0·754	0·441 0·441	−0·163 −0·163
				Amplitude $\pm 2·5°$				
0·331	1·473 1·474	1·642 1·618	0·381 0·380	0·130 0·127	1·559 1·531	0·629 0·684	0·433 0·436	−0·157 −0·157
0·385	1·465 1·440	1·583 1·521	0·376 0·370	0·117 0·114	1·531 1·543	0·675 0·625	0·419 0·427	−0·163 −0·167
0·462	1·478 1·469	1·545 1·527	0·370 0·382	0·104 0·114	1·417 1·444	0·613 0·615	0·416 0·421	−0·164 −0·175
0·576	1·480 1·502	1·517 1·477	0·372 0·379	0·106 0·091	1·415 1·420	0·657 0·629	0·416 0·422	−0·185 −0·176

TABLE 7

Results for Wing with Tip Tank

Frequency parameter ν_m	Forward axis				Rear axis			
	$(l_\theta)_f$	$(l_{\dot\theta})_f$	$(m_\theta)_f$	$(m_{\dot\theta})_f$	$(l_\theta)_r$	$(l_{\dot\theta})_r$	$(m_\theta)_r$	$(m_{\dot\theta})_r$
Amplitude $\pm 5°$								
0·331	1·339 1·333	1·488 1·403	0·392 0·389	0·103 0·086				
0·385	1·334 1·312	1·409 1·399	0·386 0·381	0·086 0·087	1·329 1·368	0·613 0·588	0·423 0·414	−0·169 −0·163
0·462	1·374 1·309	1·399 1·334	0·388 0·380	0·087 0·082	1·408 1·391	0·604 0·645	0·413 0·420	−0·157 −0·153
0·576	1·276 1·293	1·294 1·322	0·373 0·373	0·069 0·083	1·405 1·409	0·665 0·624	0·399 0·412	−0·150 −0·157
0·764	1·355 1·394	1·322 1·284	0·379 0·393	0·087 0·080	1·407 1·299	0·644 0·646	0·410 0·415	−0·155 −0·154
1·137	1·274 1·284	1·233 1·240	0·379 0·364	0·103 0·088	1·388 1·332	0·703 0·617	0·407 0·400	−0·154 −0·150
Amplitude $\pm 2·5°$								
0·331	1·297 1·310	1·461 1·449	0·373 0·372	0·088 0·092				
0·385	1·292 1·359	1·427 1·427	0·368 0·375	0·090 0·082				
0·462	1·319 1·326	1·430 1·356	0·373 0·368	0·092 0·083				
0·576	1·343 1·304	1·399 1·399	0·371 0·355	0·093 0·093				

TABLE 8

Results for Wing with Tip Tank with Rear Fin

Frequency parameter ν_m	Forward axis				Rear axis			
	$(l_\theta)_f$	$(l_{\dot\theta})_f$	$(m_\theta)_f$	$(m_{\dot\theta})_f$	$(l_\theta)_r$	$(l_{\dot\theta})_r$	$(m_\theta)_r$	$(m_{\dot\theta})_r$
			Amplitude $\pm 5°$					
0·331	1·542 1·520	1·431 1·476	0·352 0·352	0·039 0·053				
0·385	1·527 1·501	1·497 1·440	0·342 0·341	0·061 0·052	1·494 1·481	0·597 0·563	0·383 0·379	−0·162 −0·166
0·462	1·531 1·529	1·464 1·441	0·349 0·347	0·060 0·045	1·467 1·457	0·628 0·528	0·380 0·372	−0·153 −0·155
0·576	1·537 1·589	1·435 1·364	0·355 0·347	0·057 0·051	1·523 1·501	0·625 0·568	0·378 0·378	−0·155 −0·159
0·764	1·598 1·594	1·356 1·429	0·340 0·364	0·049 0·073	1·412 1·452	0·621 0·615	0·376 0·362	−0·164 −0·156
1·137	1·640 1·600	1·477 1·449	0·376 0·344	0·100 0·087	1·286 1·414	0·658 0·644	0·346 0·350	−0·159 −0·145
			Amplitude $\pm 2·5°$					
0·331	1·471 1·476	1·503 1·515	0·334 0·333	0·074 0·069				
0·385	1·448 1·479	1·456 1·466	0·331 0·334	0·067 0·065				
0·462	1·438 1·467	1·347 1·495	0·328 0·321	0·055 0·071				
0·576	1·547 1·545	1·275 1·366	0·343 0·337	0·051 0·058				

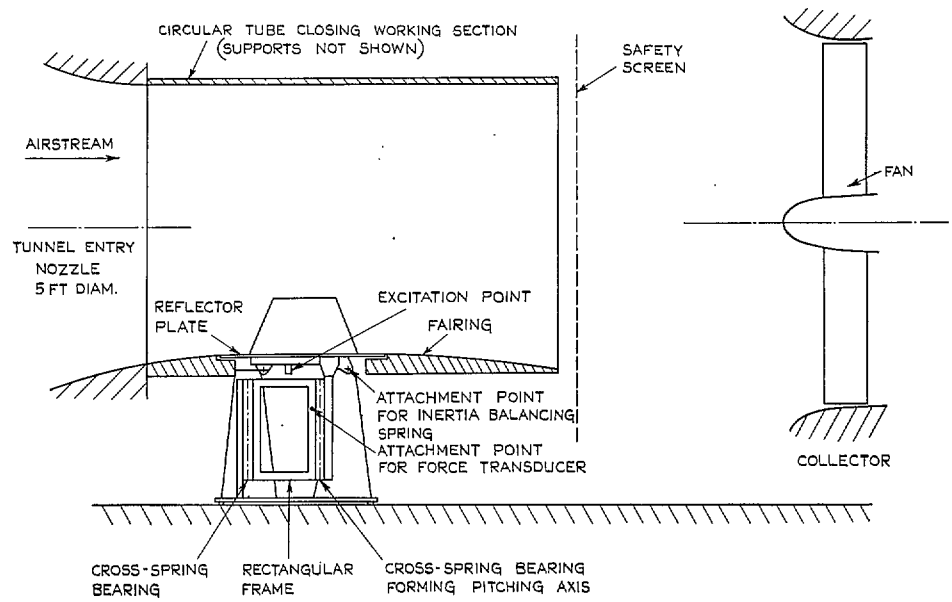

FIG. 1. Arrangement of wing in wind-tunnel working section.

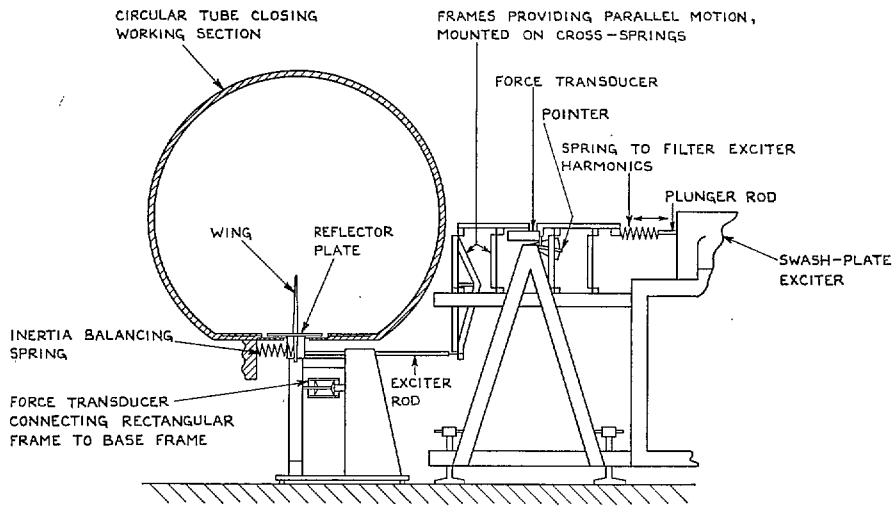

FIG. 2. Arrangement of wing and excitation equipment in wind-tunnel working section.

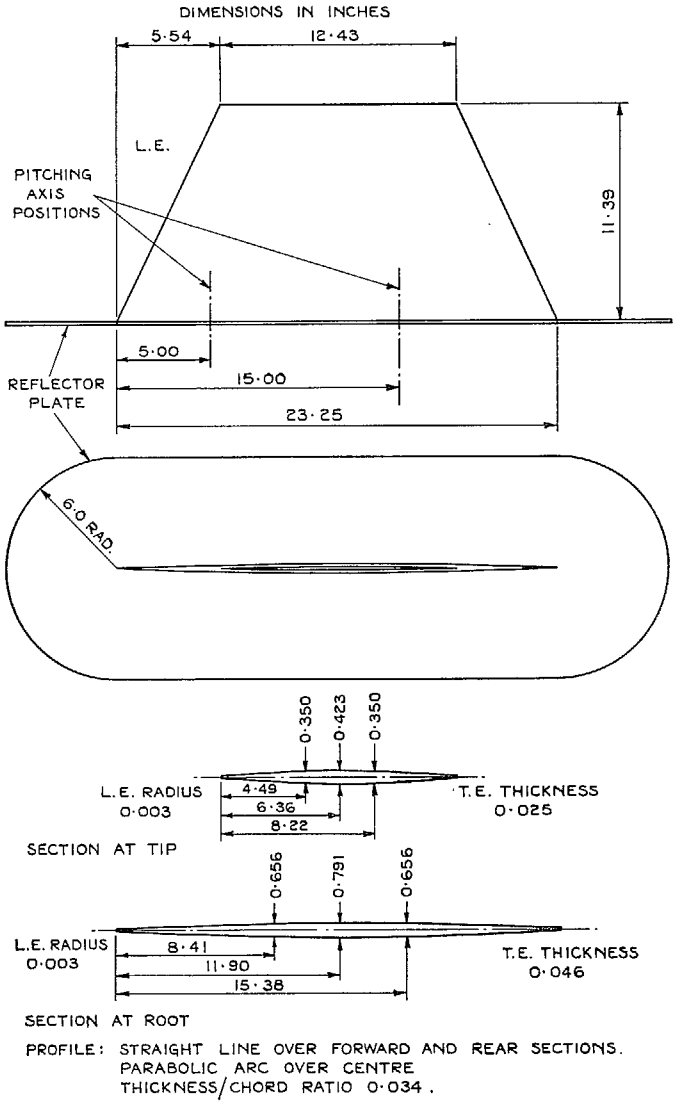

FIG. 3. Wing dimensions.

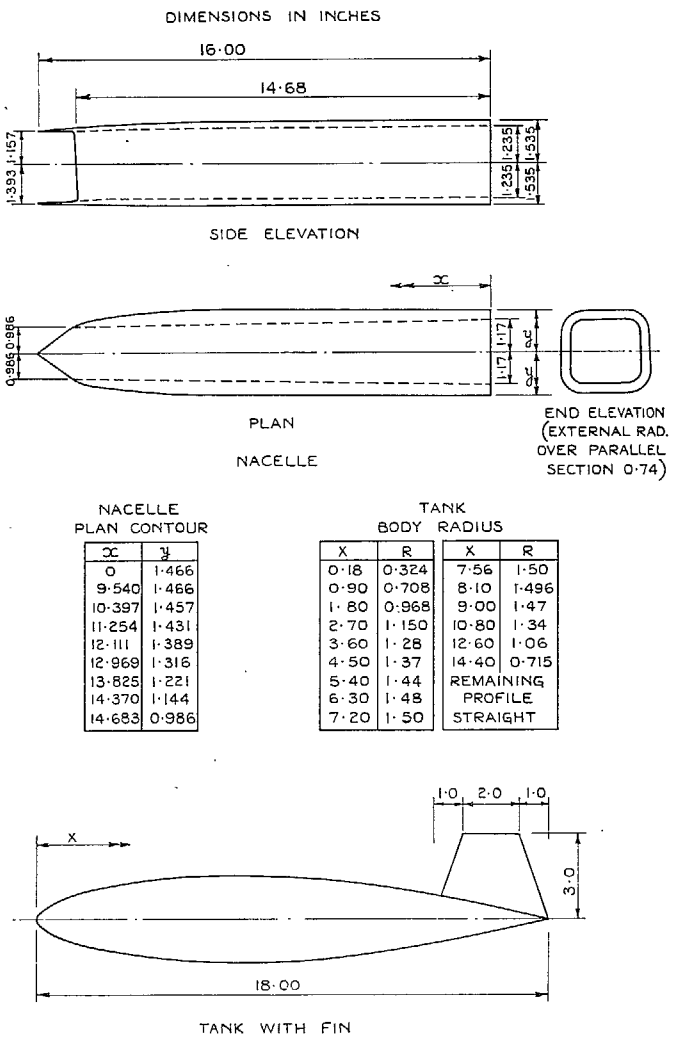

x	y
0	1·466
9·540	1·466
10·397	1·457
11·254	1·431
12·111	1·389
12·969	1·316
13·825	1·221
14·370	1·144
14·683	0·986

X	R	X	R
0·18	0·324	7·56	1·50
0·90	0·708	8·10	1·496
1·80	0·968	9·00	1·47
2·70	1·150	10·80	1·34
3·60	1·28	12·60	1·06
4·50	1·37	14·40	0·715
5·40	1·44	REMAINING PROFILE STRAIGHT	
6·30	1·48		
7·20	1·50		

FIG. 4. Nacelle and tank dimensions.

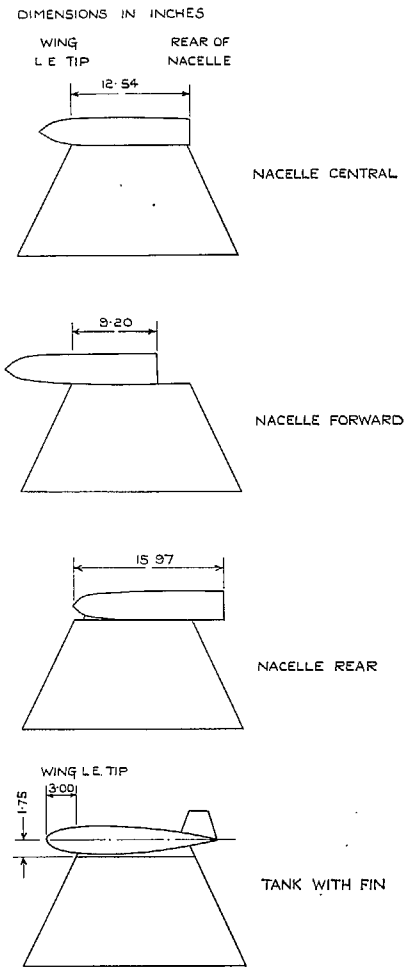

FIG. 5. Nacelle and tank positions.

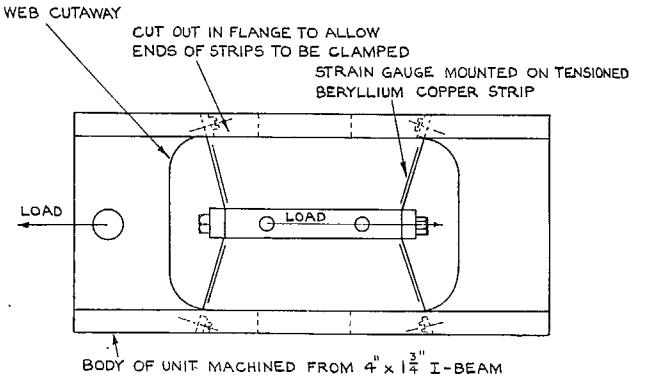

FIG. 6. Force transducer.

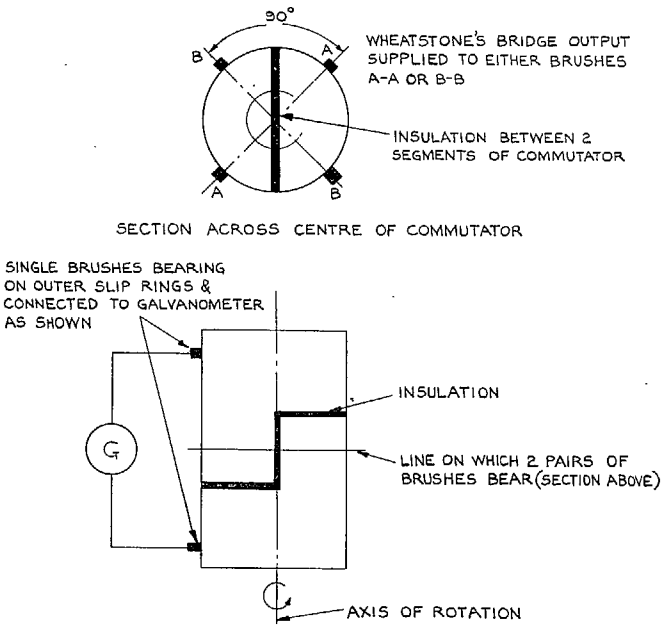

FIG. 7. Commutator and brush arrangement.

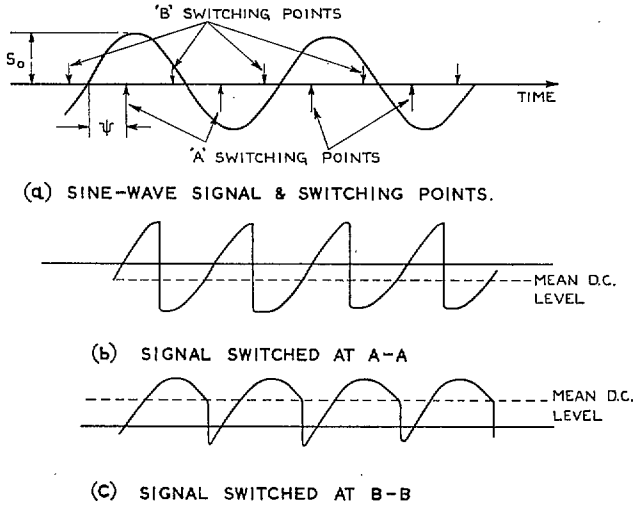

FIG. 8a to c. Transducer output signal and switching.

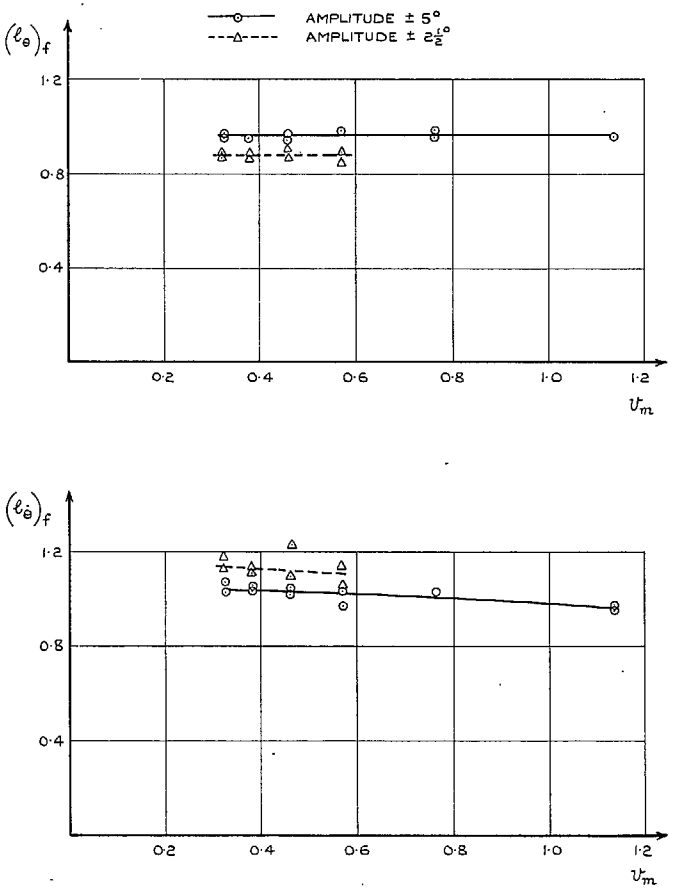

FIG. 9. Variation of $(l_\theta)_f$ and $(l_{\dot\theta})_f$ with frequency parameter: plain wing.

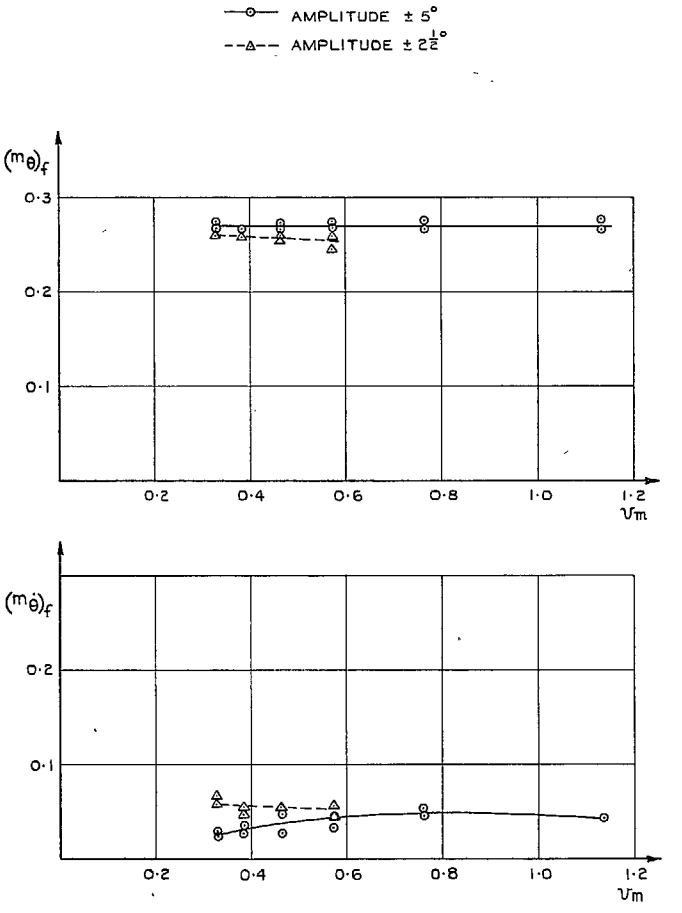

FIG. 10. Variation of $(m_\theta)_f$ and $(m_{\dot\theta})_f$ with frequency parameter: plain wing.

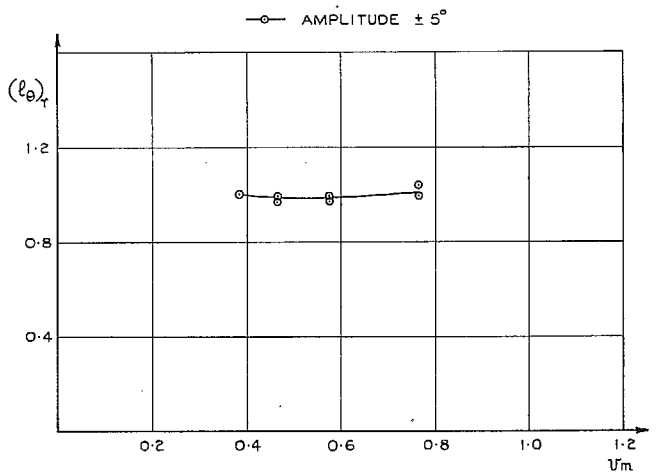

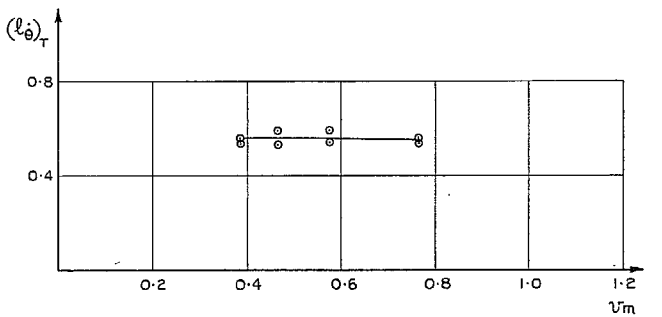

FIG. 11. Variation of $(l_\theta)_r$ and $(l_{\dot\theta})_r$ with frequency parameter: plain wing.

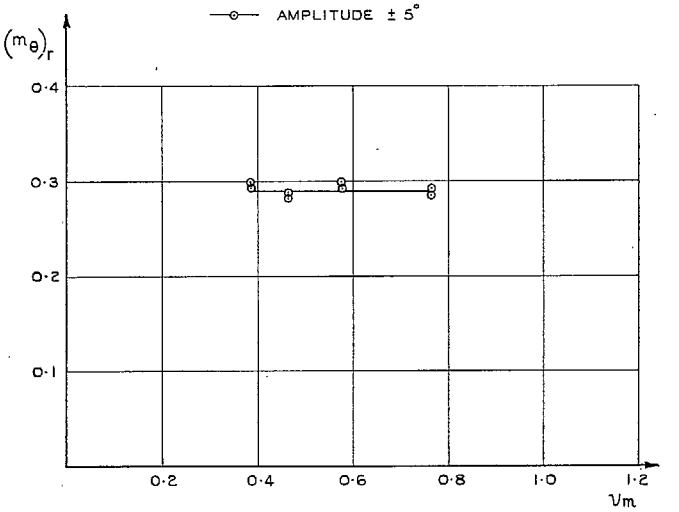

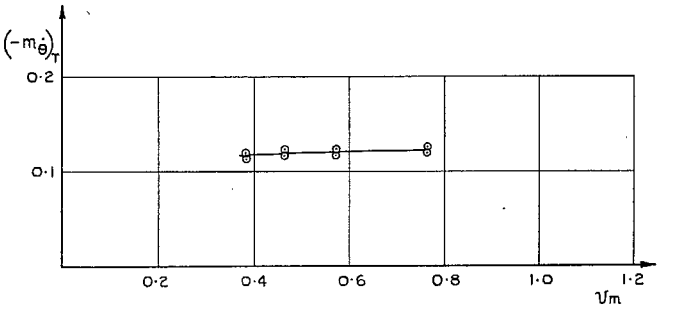

FIG. 12. Variation of $(m_\theta)_r$ and $(-m_{\dot\theta})_r$ with frequency parameter: plain wing.

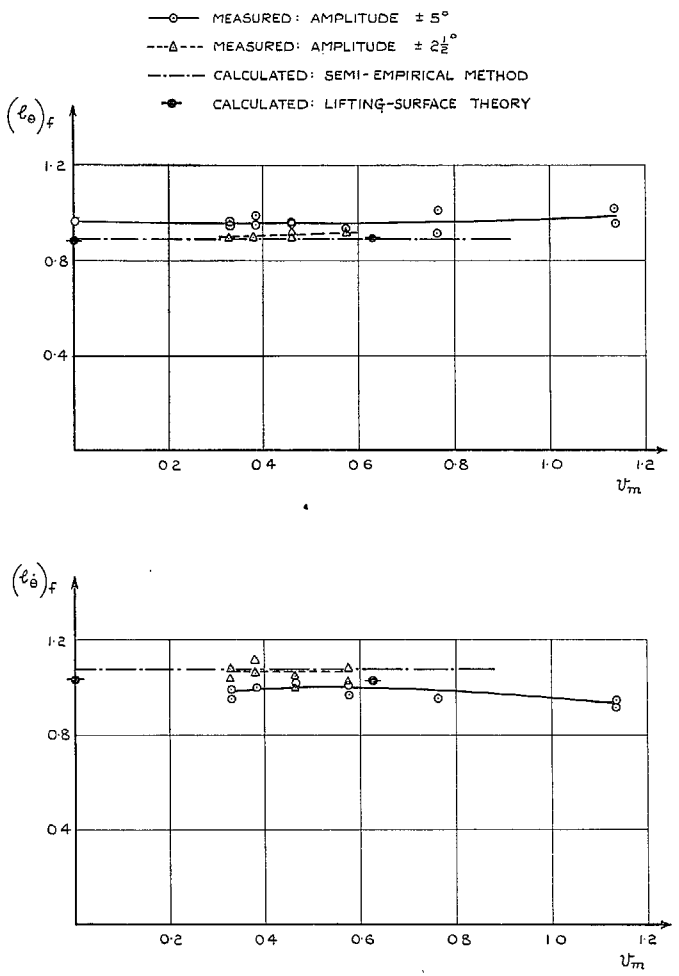

FIG. 13. Variation of $(l_\theta)_f$ and $(l_{\dot\theta})_f$ with frequency parameter: wing with transition wire.

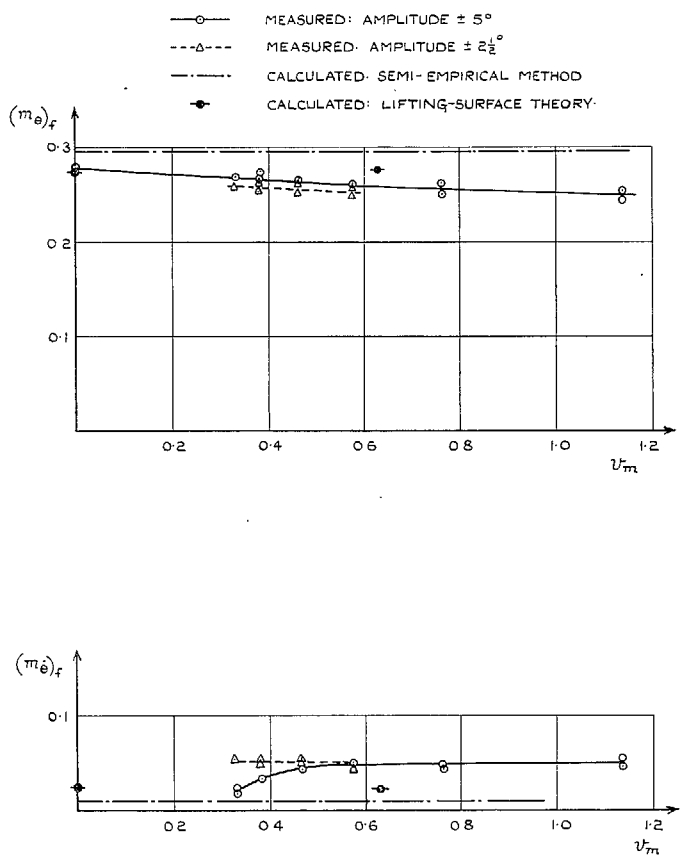

FIG. 14. Variation of $(m_\theta)_f$ and $(m_{\dot\theta})_f$ with frequency parameter: wing with transition wire.

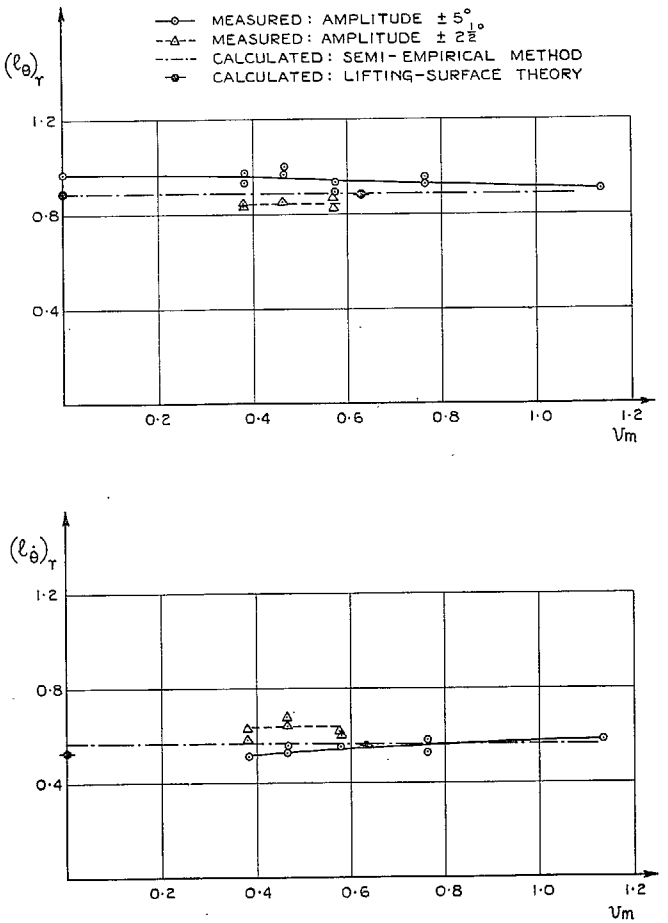

FIG. 15. Variation of $(l_\theta)_r$ and $(l_{\dot\theta})_r$ with frequency parameter: wing with transition wire.

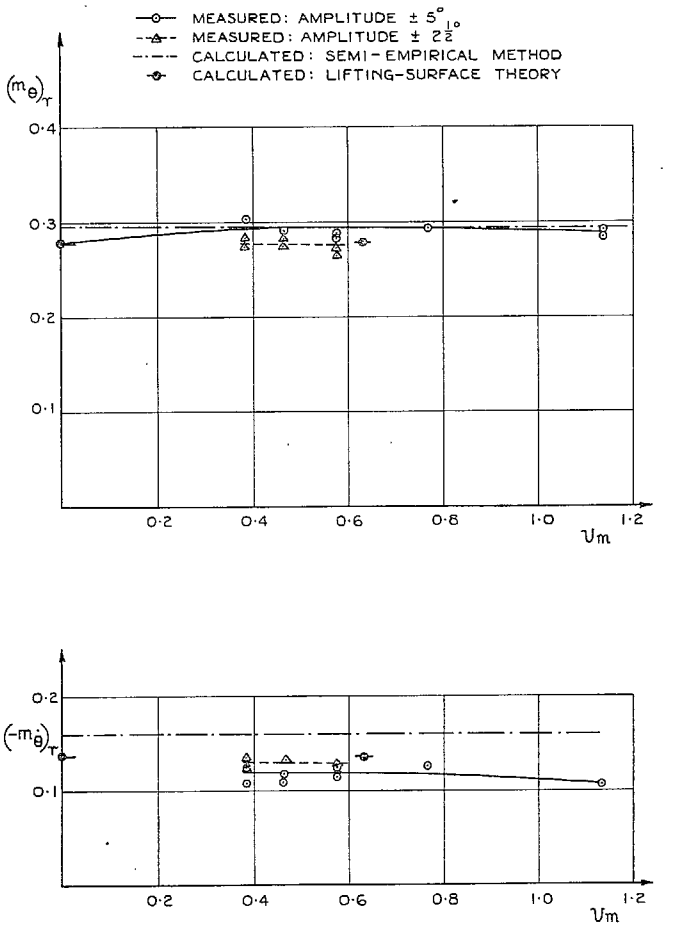

FIG. 16. Variation of $(m_\theta)_r$ and $(-m_{\dot\theta})_r$ with frequency parameter: wing with transition wire.

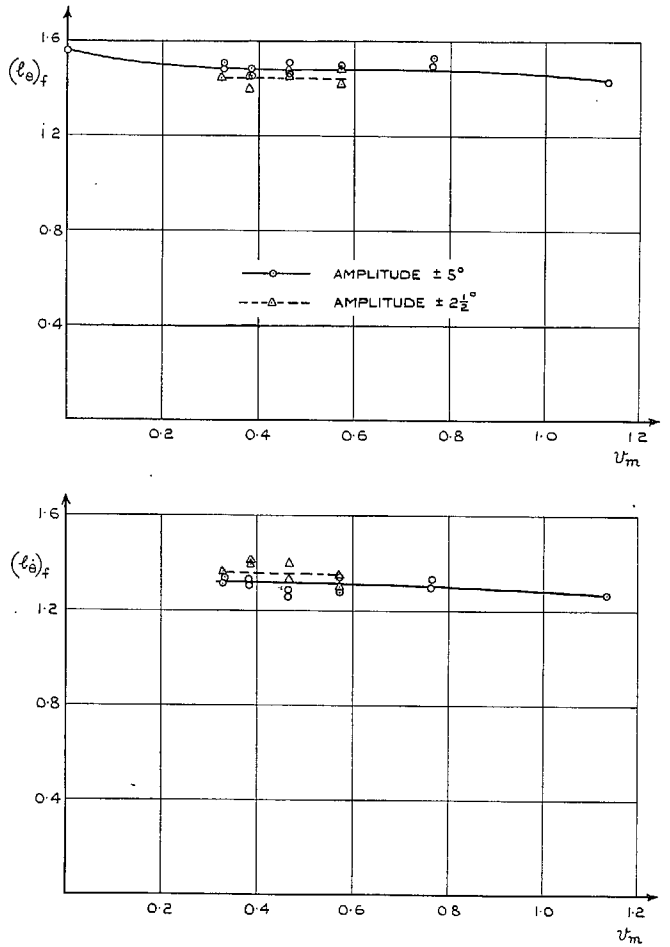

FIG. 17. Variation of $(l_\theta)_f$ and $(l_{\dot\theta})_f$ with frequency parameter: nacelle forward.

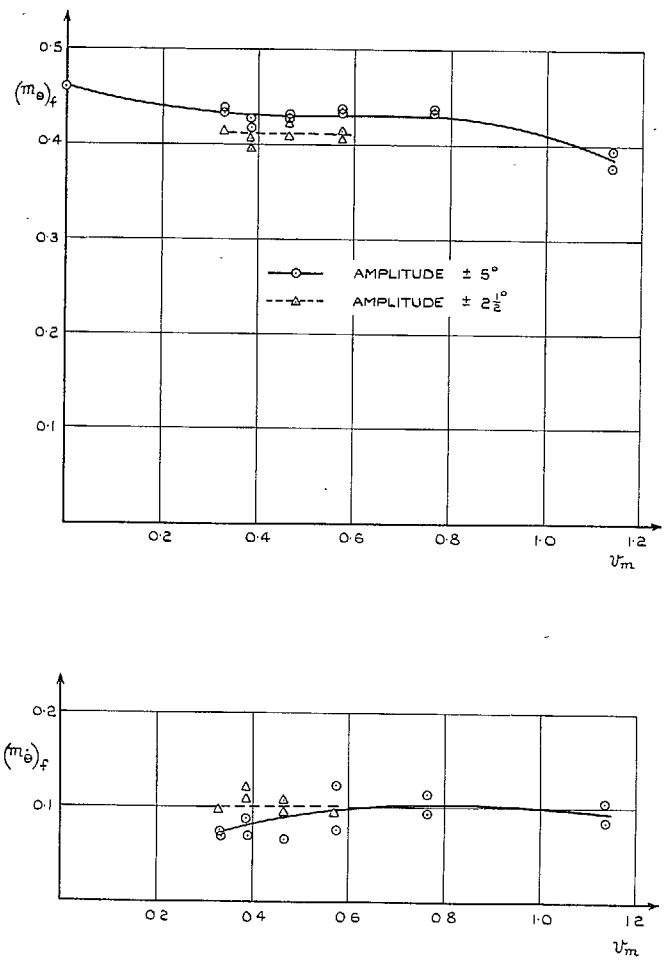

FIG. 18. Variation of $(m_\theta)_f$ and $(m_{\dot\theta})_f$ with frequency parameter: nacelle forward.

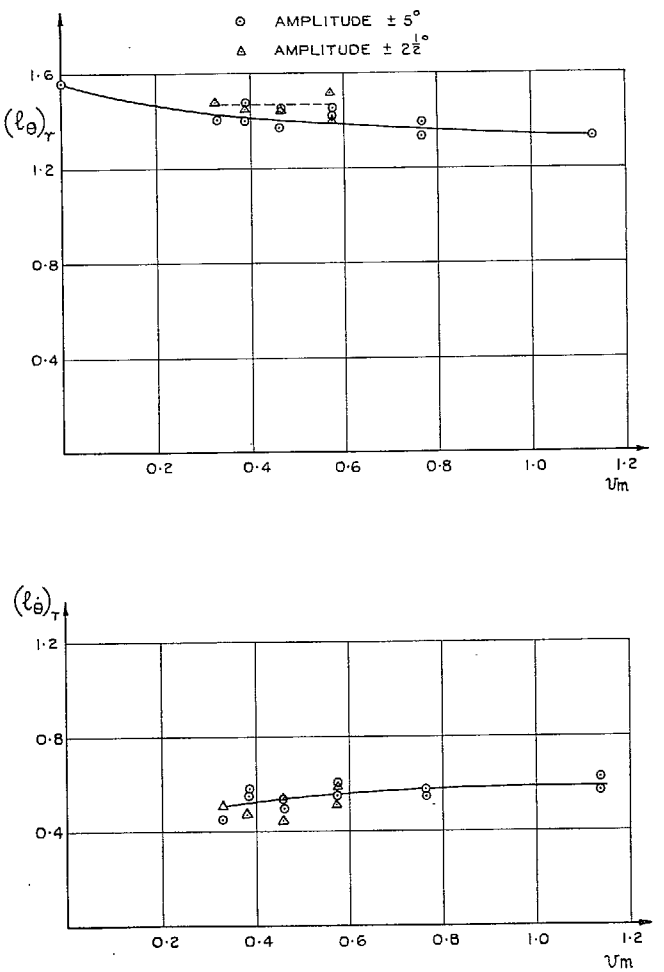

FIG. 19. Variation of $(l_\theta)_r$ and $(l_{\dot\theta})_r$ with frequency parameter: nacelle forward.

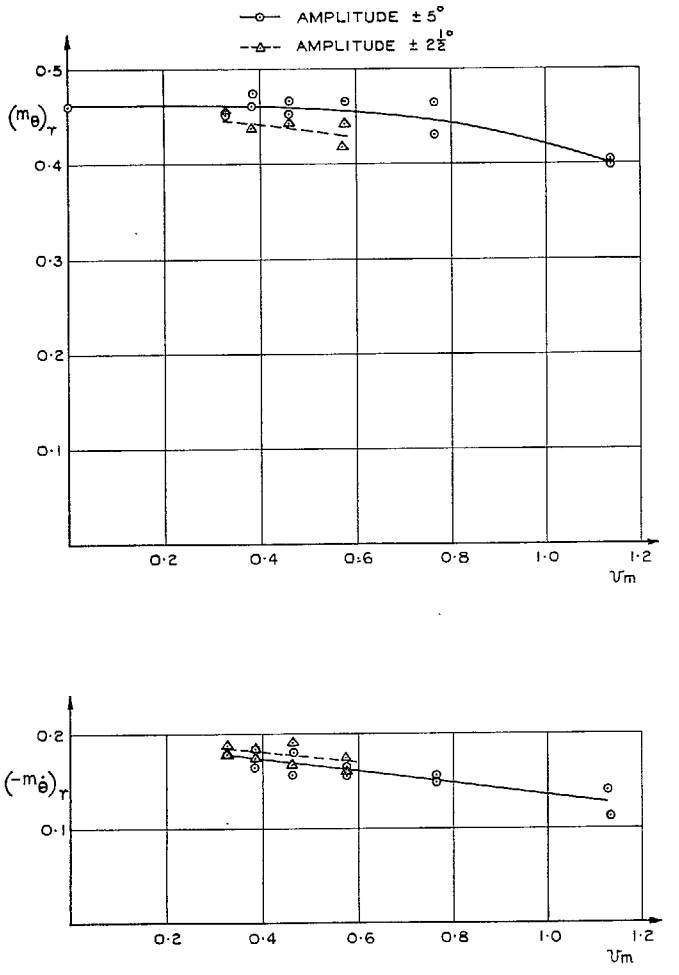

FIG. 20. Variation of $(m_\theta)_r$ and $(-m_{\dot\theta})_r$ with frequency parameter: nacelle forward.

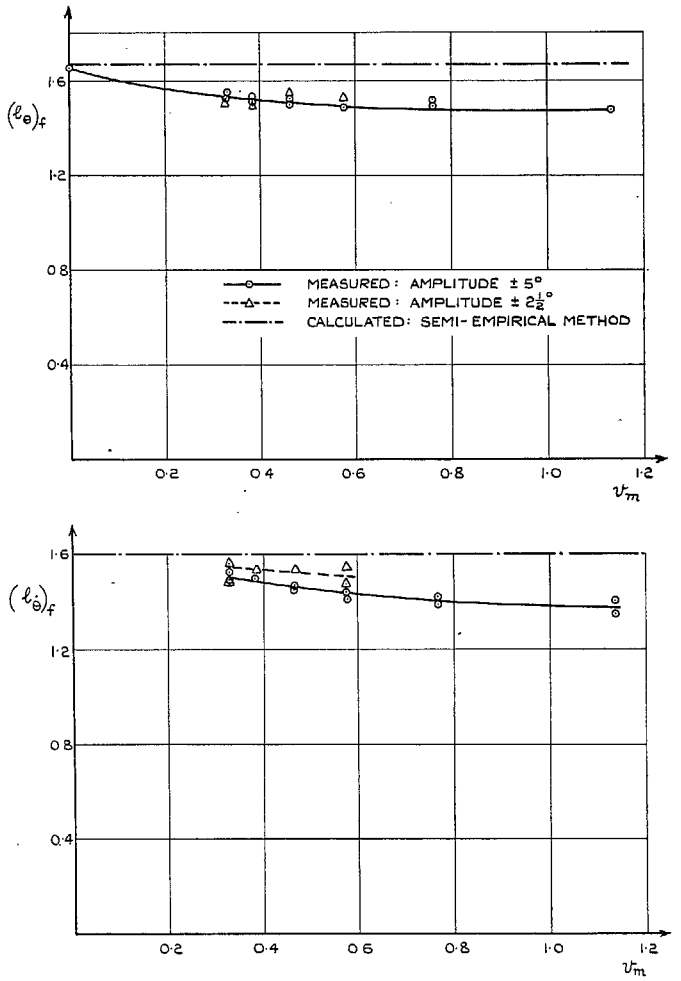

FIG. 21. Variation of $(l_\theta)_f$ and $(l_{\dot\theta})_f$ with frequency parameter: nacelle central.

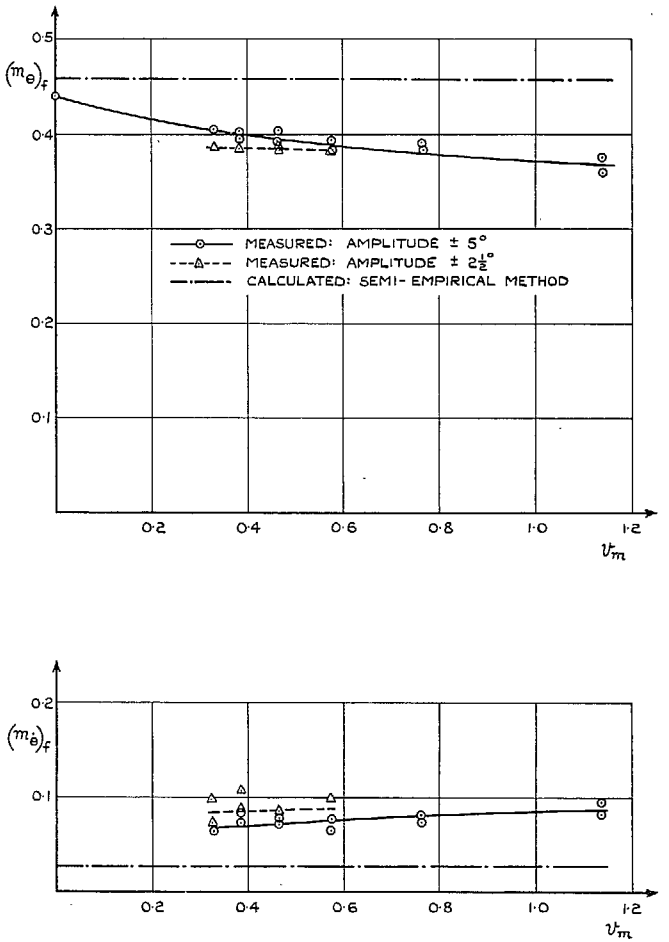

FIG. 22. Variation of $(m_\theta)_f$ and $(m_{\dot\theta})_f$ with frequency parameter: nacelle central.

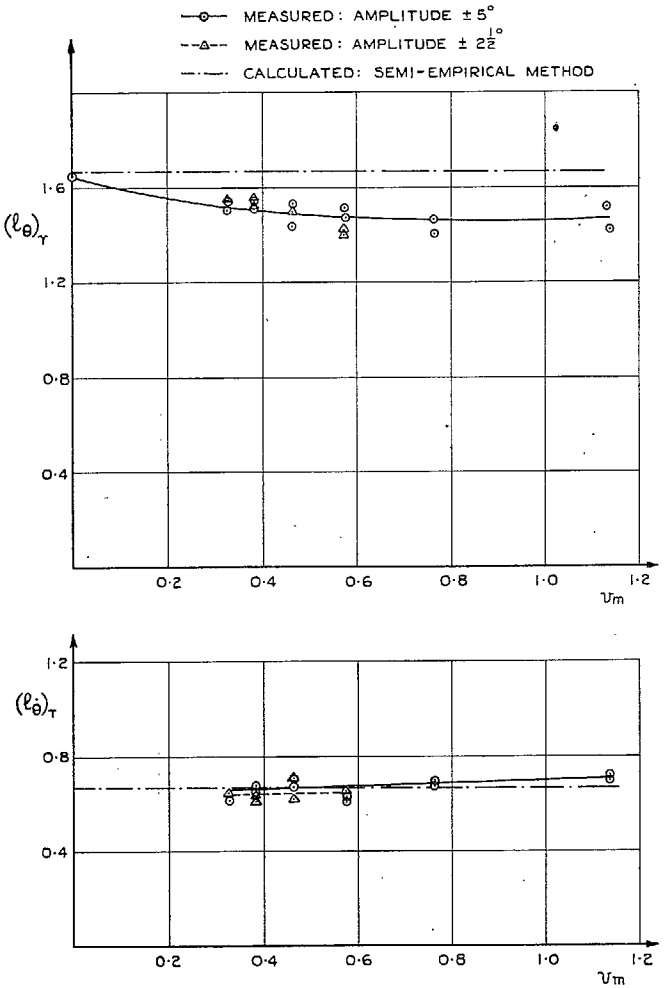

FIG. 23. Variation of $(l_\theta)_r$ and $(l_{\dot\theta})_r$ with frequency parameter: nacelle central.

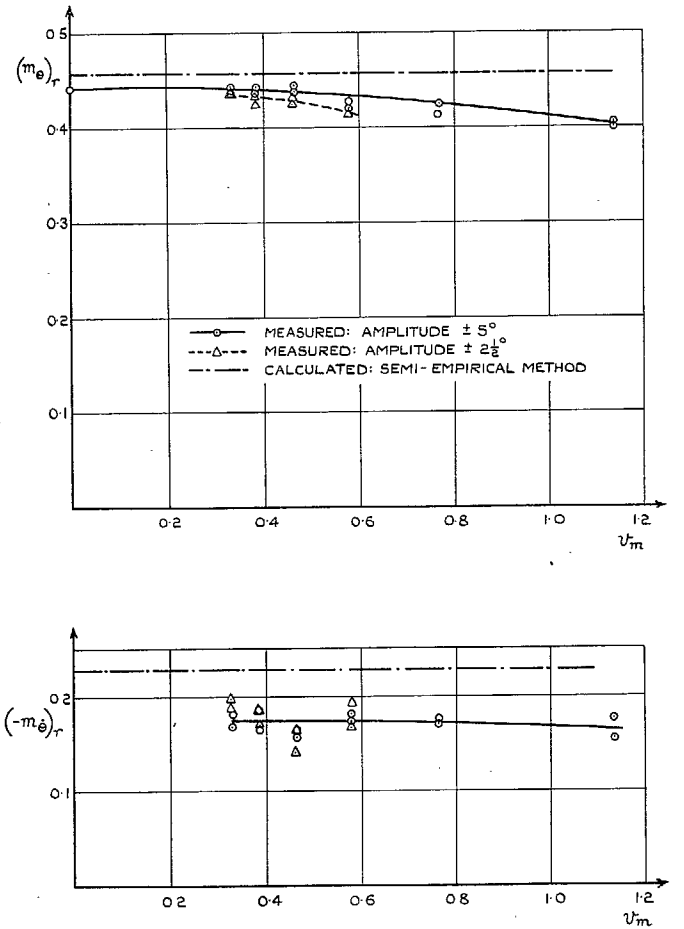

FIG. 24. Variation of $(m_\theta)_r$ and $(-m_{\dot\theta})_r$ with frequency parameter: nacelle central.

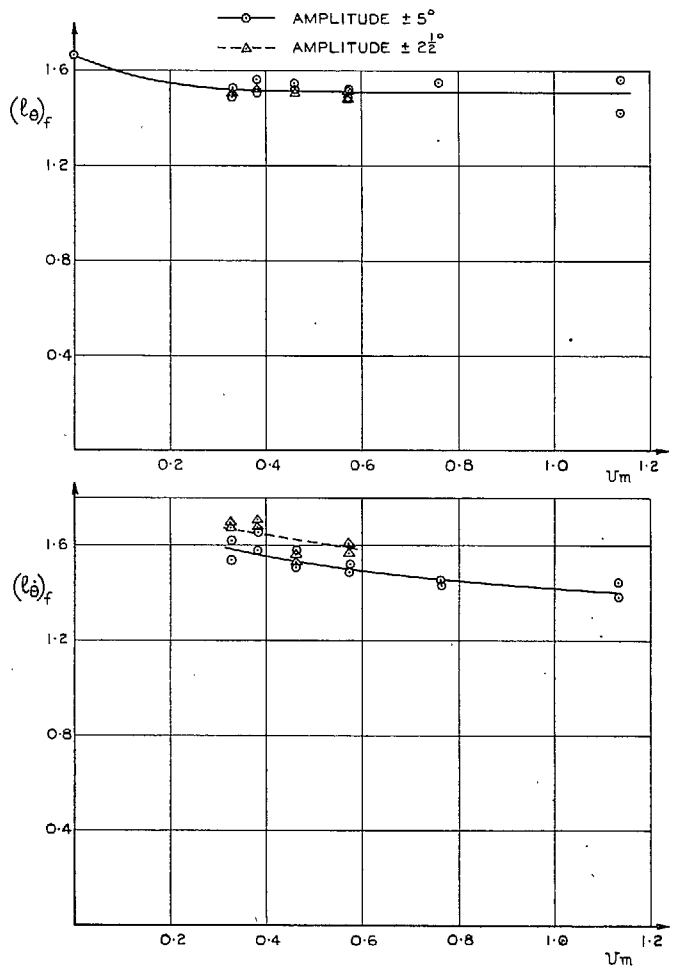

FIG. 25. Variation of $(l_\theta)_f$ and $(l_{\dot\theta})_f$ with frequency parameter: nacelle rear.

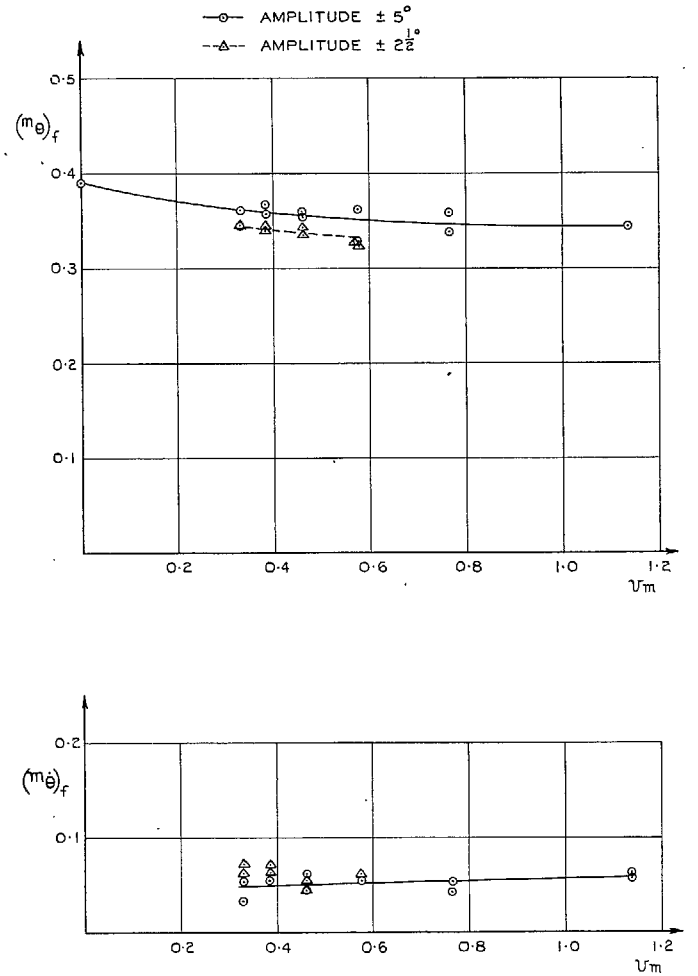

FIG. 26. Variation of $(m_\theta)_f$ and $(m_{\dot\theta})_f$ with frequency parameter: nacelle rear.

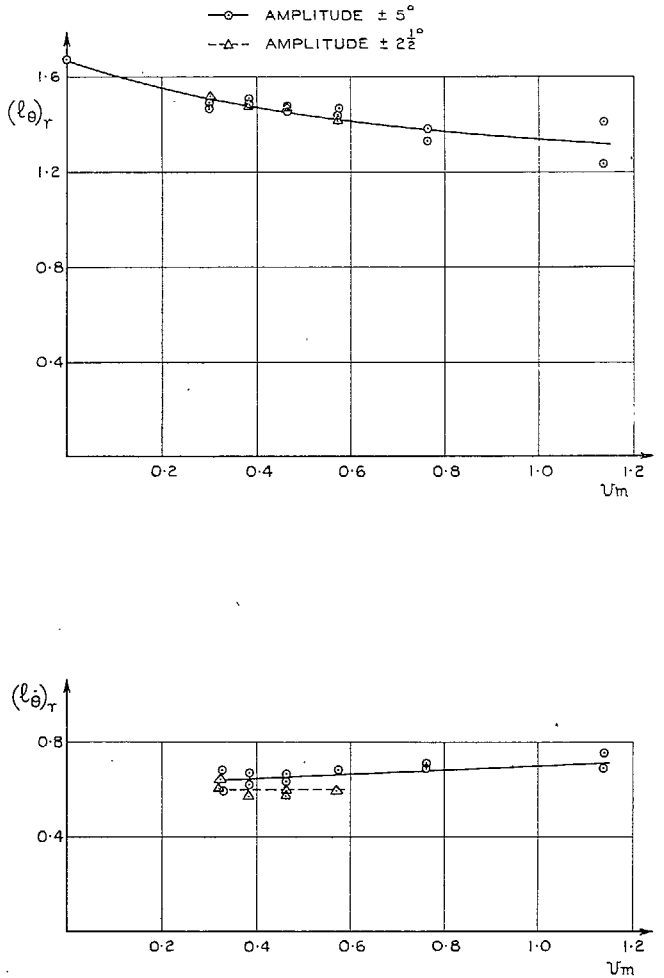

FIG. 27. Variation of $(l_\theta)_r$ and $(l_{\dot\theta})_r$ with frequency parameter: nacelle rear.

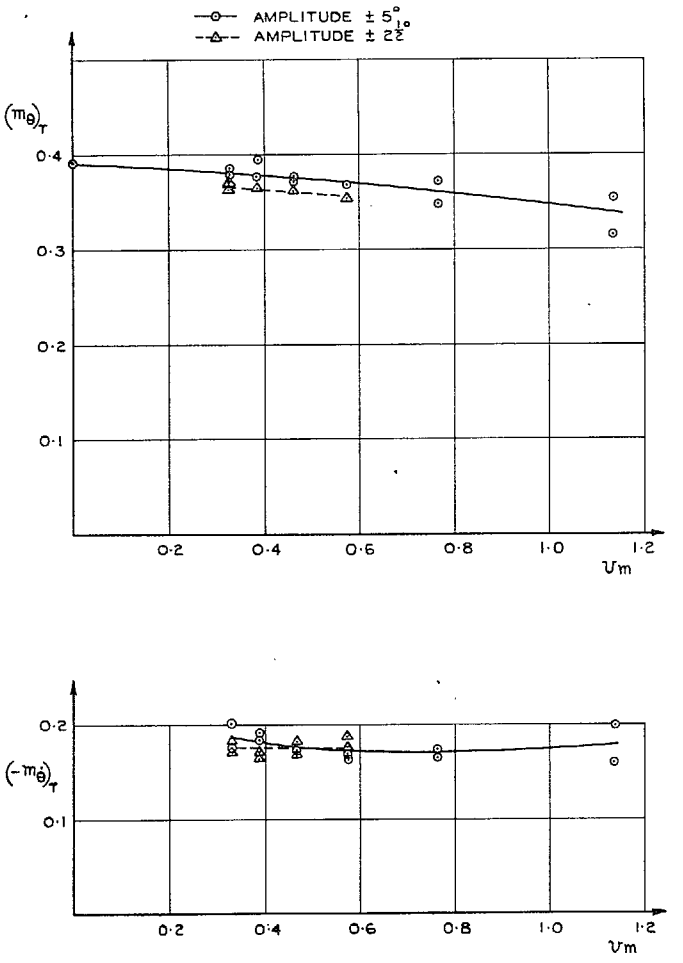

FIG. 28. Variation of $(m_\theta)_r$ and $(-m_{\dot\theta})_r$ with frequency parameter: nacelle rear.

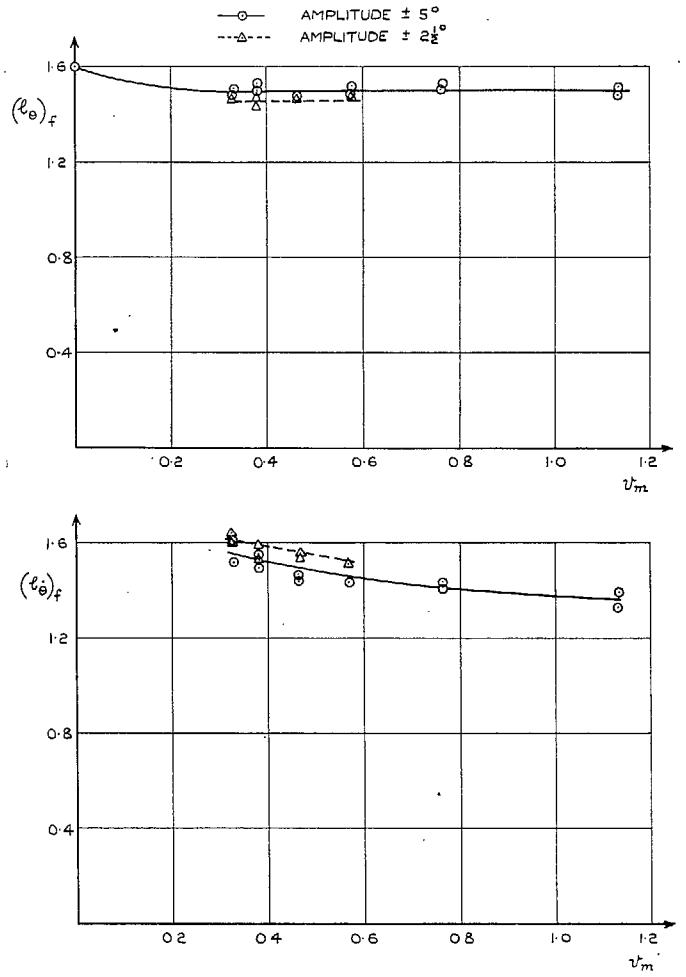

FIG. 29. Variation of $(l_\theta)_f$ and $(l_{\dot\theta})_f$ with frequency parameter: nacelle central, rear blocked.

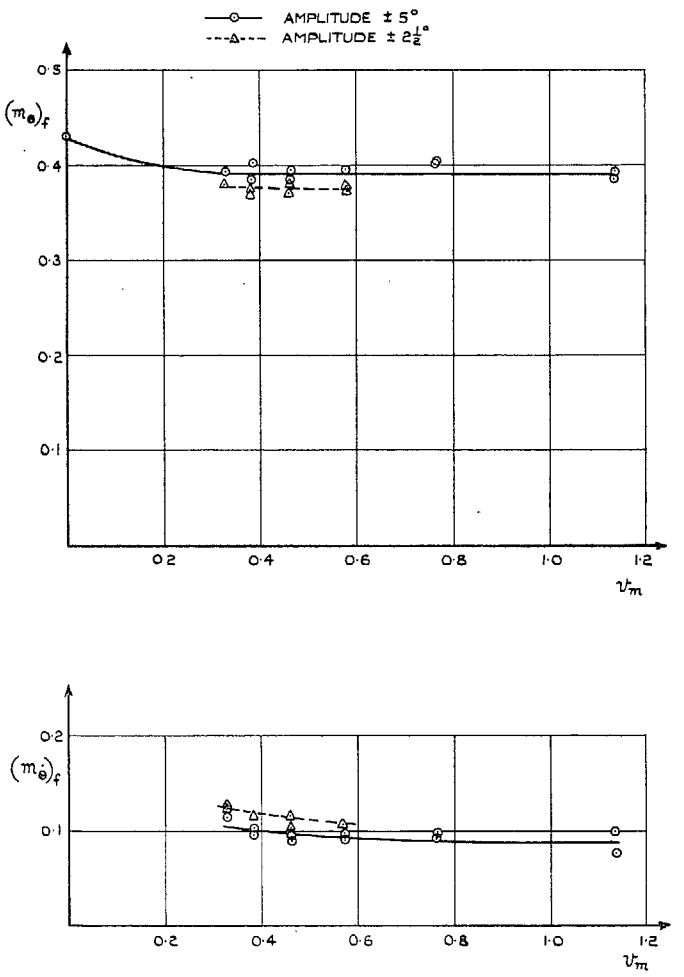

FIG. 30. Variation of $(m_\theta)_f$ and $(m_{\dot\theta})_f$ with frequency parameter: nacelle central, rear blocked.

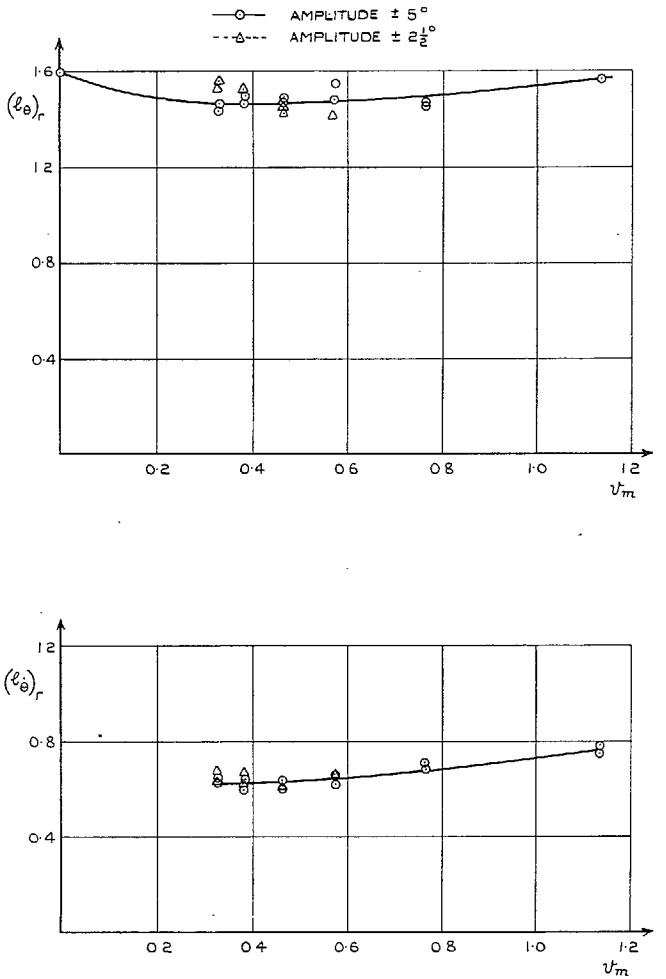

FIG. 31. Variation of $(l_\theta)_r$ and $(l_{\dot\theta})_r$ with frequency parameter: nacelle central, rear blocked.

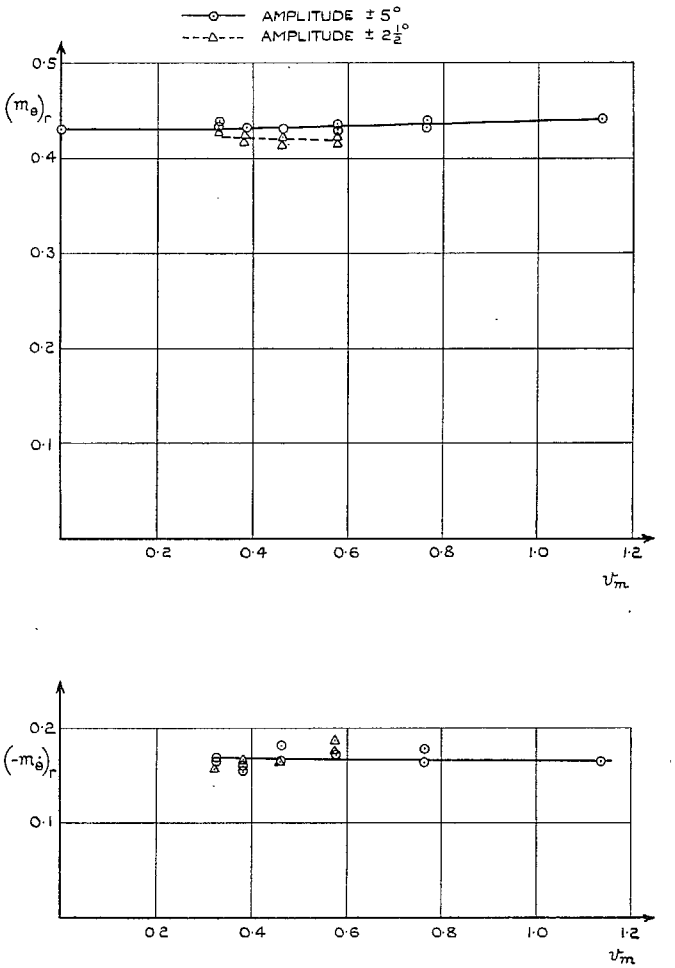

FIG. 32. Variation of $(m_\theta)_r$ and $(-m_{\dot\theta})_r$ with frequency parameter: nacelle central, rear blocked.

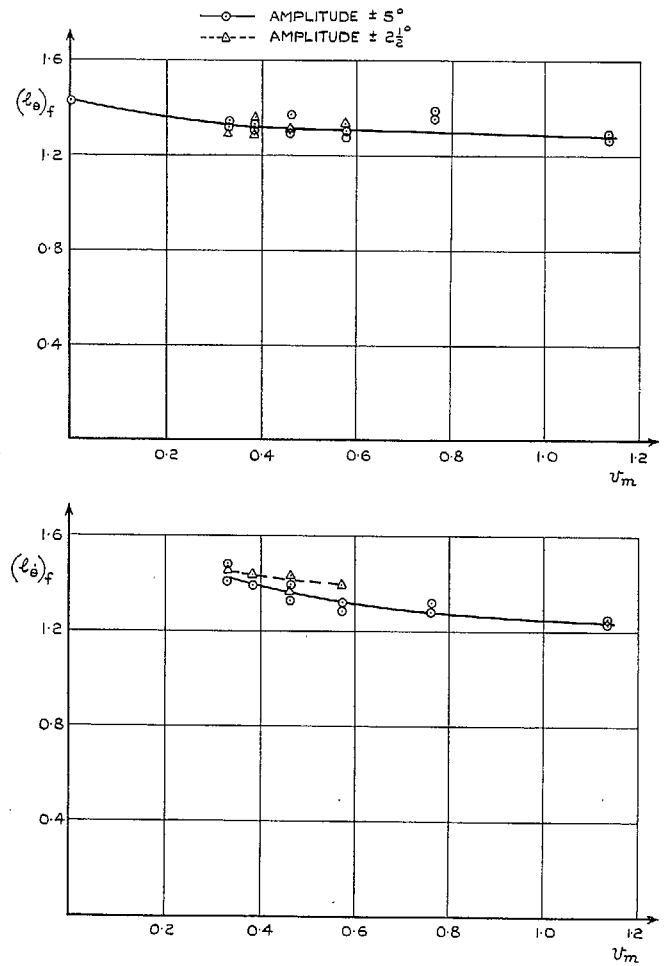

FIG. 33. Variation of $(l_\theta)_f$ and $(l_{\dot\theta})_f$ with frequency parameter: tip tank fitted.

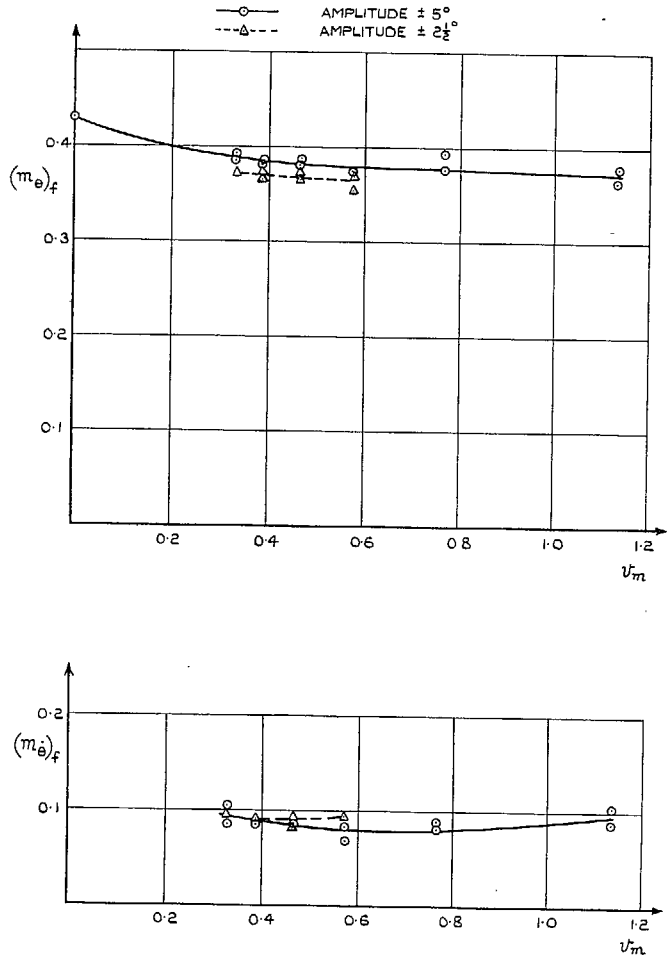

FIG. 34. Variation of $(m_\theta)_f$ and $(m_{\dot\theta})_f$ with frequency parameter: tip tank fitted.

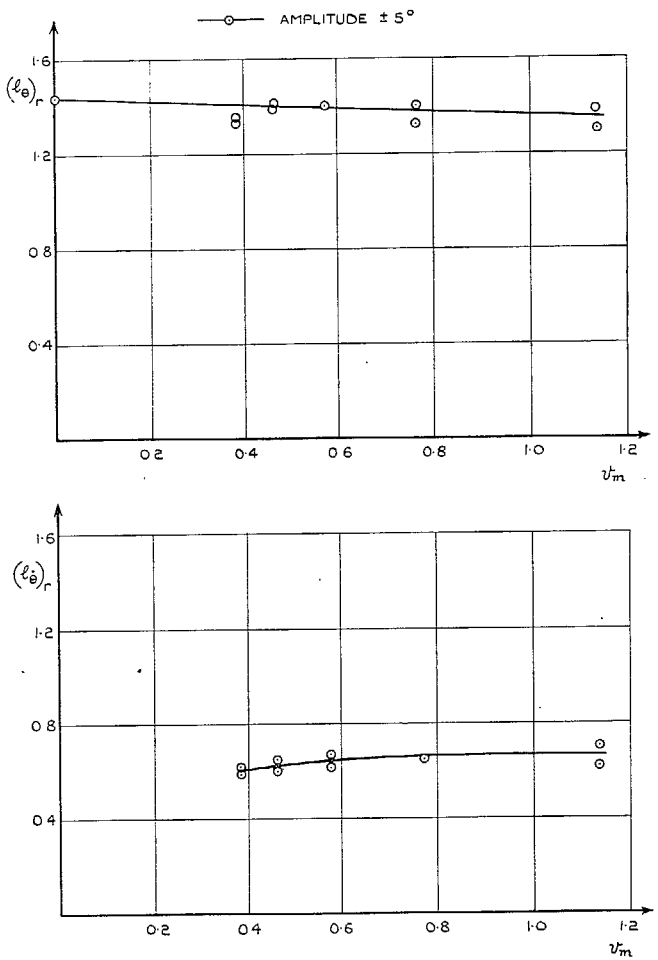

FIG. 35. Variation of $(l_\theta)_r$ and $(l_{\dot\theta})_r$ with frequency parameter: tip tank fitted.

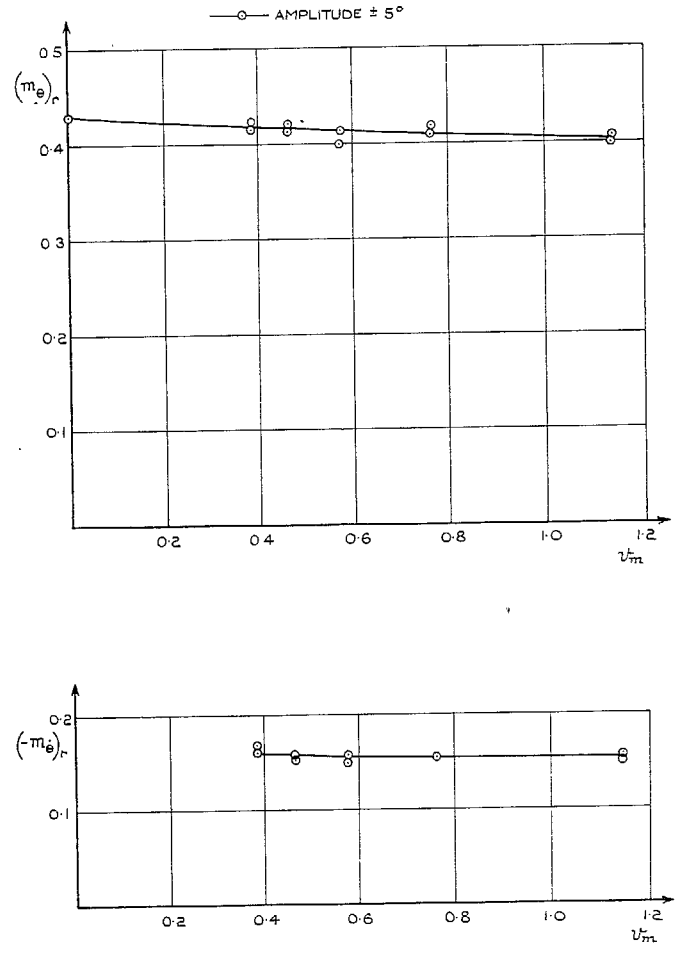

FIG. 36. Variation of $(m_\theta)_r$ and $(-m_{\dot\theta})_r$ with frequency parameter: tip tank fitted.

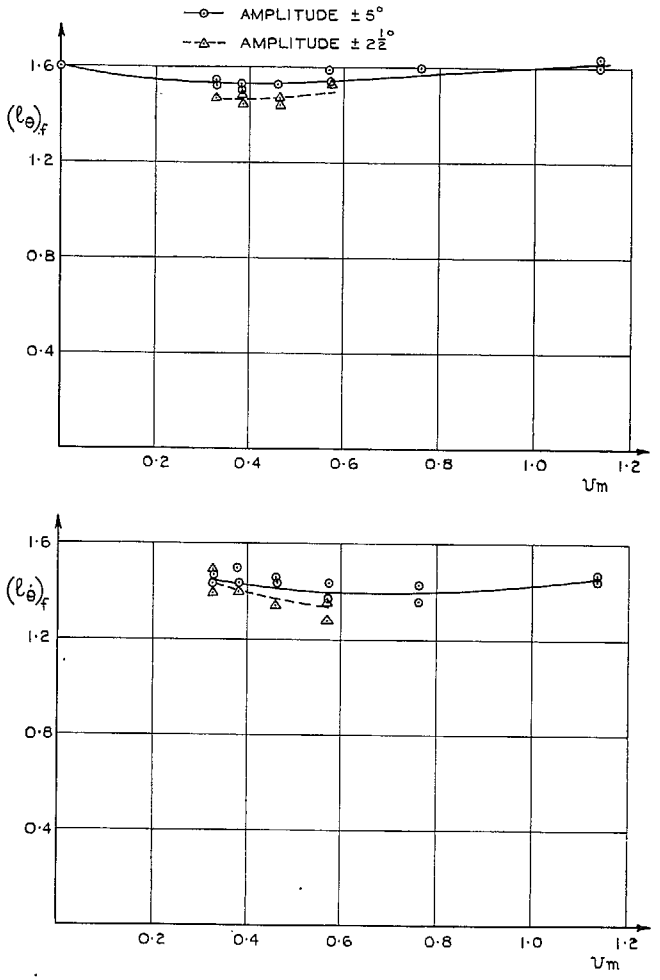

FIG. 37. Variation of $(l_\theta)_f$ and $(l_{\dot\theta})_f$ with frequency parameter: wing with tip tank with rear fin.

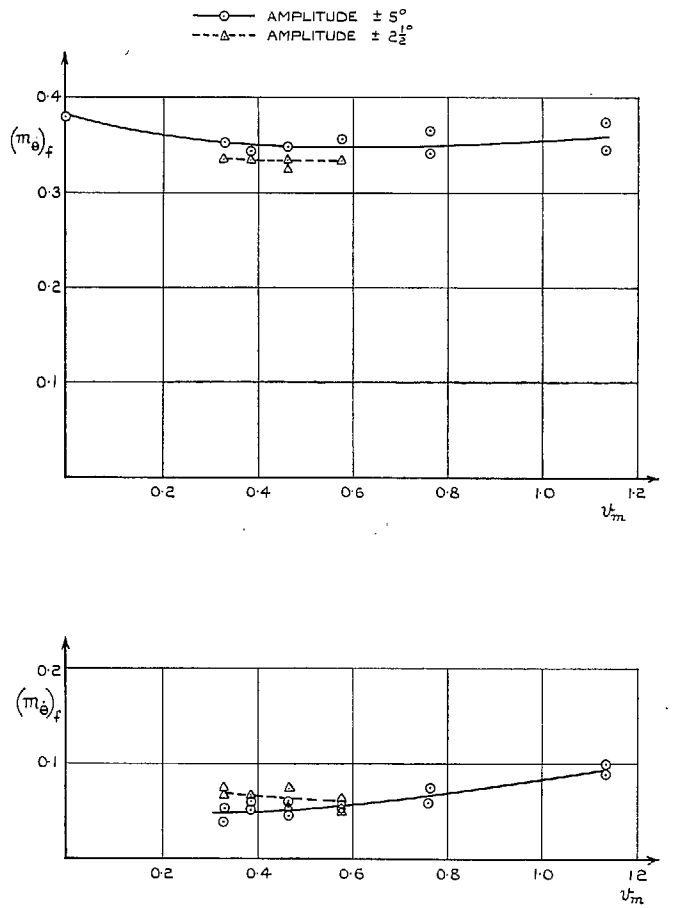

FIG. 38. Variation of $(m_\theta)_f$ and $(m_{\dot\theta})_f$ with frequency parameter: wing with tip tank with rear fin.

(90071) Wt. 66/2301 K.5 9/64 Hw.

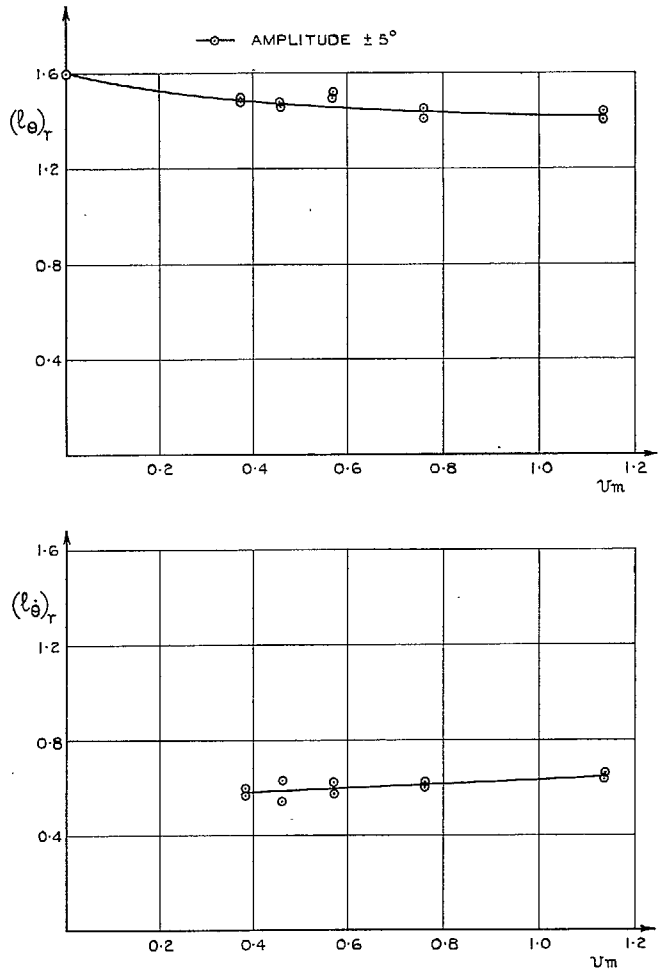

FIG. 39. Variation of $(l_\theta)_r$ and $(l_{\dot\theta})_r$ with frequency parameter: wing with tip tank with rear fin.

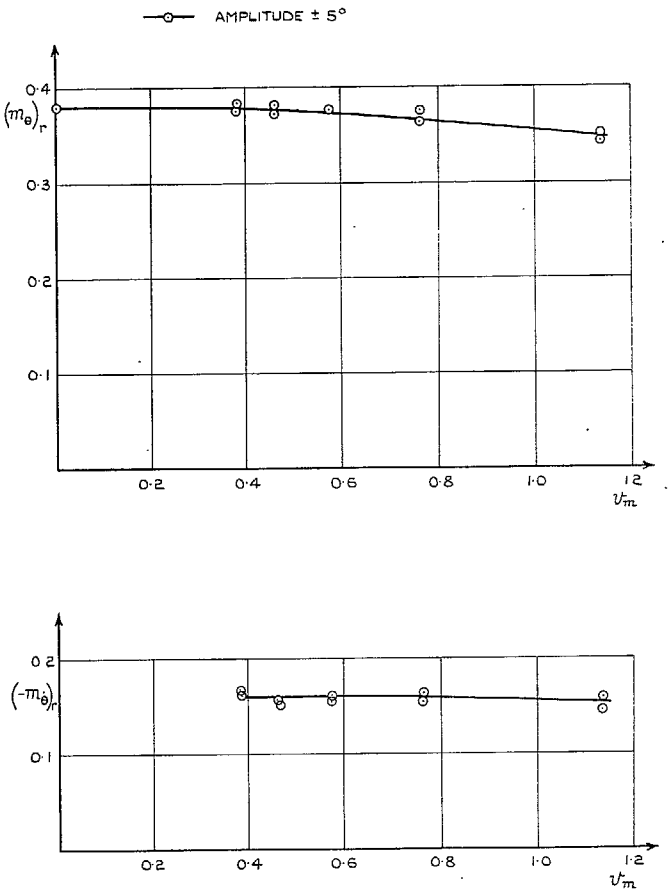

FIG. 40. Variation of $(m_\theta)_r$ and $(-m_{\dot\theta})_r$ with frequency parameter: wing with tip tank with rear fin.

Publications of the Aeronautical Research Council

ANNUAL TECHNICAL REPORTS OF THE AERONAUTICAL RESEARCH COUNCIL (BOUND VOLUMES)

1942 Vol. I. Aero and Hydrodynamics, Aerofoils, Airscrews, Engines. 75*s.* (post 2*s.* 9*d.*)
Vol. II. Noise, Parachutes, Stability and Control, Structures, Vibration, Wind Tunnels. 47*s.* 6*d.* (post 2*s.* 3*d.*)

1943 Vol. I. Aerodynamics, Aerofoils, Airscrews. 80*s.* (post 2*s.* 6*d.*)
Vol. II. Engines, Flutter, Materials, Parachutes, Performance, Stability and Control, Structures. 90*s.* (post 2*s.* 9*d.*)

1944 Vol. I. Aero and Hydrodynamics, Aerofoils, Aircraft, Airscrews, Controls. 84*s.* (post 3*s.*)
Vol. II. Flutter and Vibration, Materials, Miscellaneous, Navigation, Parachutes, Performance, Plates and Panels, Stability, Structures, Test Equipment, Wind Tunnels. 84*s.* (post 3*s.*)

1945 Vol. I. Aero and Hydrodynamics, Aerofoils. 130*s.* (post 3*s.* 6*d.*)
Vol. II. Aircraft, Airscrews, Controls. 130*s.* (post 3*s.* 6*d.*)
Vol. III. Flutter and Vibration, Instruments, Miscellaneous, Parachutes, Plates and Panels, Propulsion. 130*s.* (post 3*s.* 3*d.*)
Vol. IV. Stability, Structures, Wind Tunnels, Wind Tunnel Technique. 130*s.* (post 3*s.* 3*d.*)

1946 Vol. I. Accidents, Aerodynamics, Aerofoils and Hydrofoils. 168*s.* (post 3*s.* 9*d.*)
Vol. II. Airscrews, Cabin Cooling, Chemical Hazards, Controls, Flames, Flutter, Helicopters, Instruments and Instrumentation, Interference, Jets, Miscellaneous, Parachutes. 168*s.* (post 3*s.* 3*d.*)
Vol. III. Performance, Propulsion, Seaplanes, Stability, Structures, Wind Tunnels. 168*s.* (post 3*s.* 6*d.*)

1947 Vol. I. Aerodynamics, Aerofoils, Aircraft. 168*s.* (post 3*s.* 9*d.*)
Vol. II. Airscrews and Rotors, Controls, Flutter, Materials, Miscellaneous, Parachutes, Propulsion, Seaplanes, Stability, Structures, Take-off and Landing. 168*s.* (post 3*s.* 9*d.*)

1948 Vol. I. Aerodynamics, Aerofoils, Aircraft, Airscrews, Controls, Flutter and Vibration, Helicopters, Instruments, Propulsion, Seaplane, Stability, Structures, Wind Tunnels. 130*s.* (post 3*s.* 3*d.*)
Vol. II. Aerodynamics, Aerofoils, Aircraft, Airscrews, Controls, Flutter and Vibration, Helicopters, Instruments, Propulsion, Seaplane, Stability, Structures, Wind Tunnels. 110*s.* (post 3*s.* 3*d.*)

Special Volumes

Vol. I. Aero and Hydrodynamics, Aerofoils, Controls, Flutter, Kites, Parachutes, Performance, Propulsion, Stability. 126*s.* (post 3*s.*)
Vol. II. Aero and Hydrodynamics, Aerofoils, Airscrews, Controls, Flutter, Materials, Miscellaneous, Parachutes, Propulsion, Stability, Structures. 147*s.* (post 3*s.*)
Vol. III. Aero and Hydrodynamics, Aerofoils, Airscrews, Controls, Flutter, Kites, Miscellaneous, Parachutes, Propulsion, Seaplanes, Stability, Structures, Test Equipment. 189*s.* (post 3*s.* 9*d.*)

Reviews of the Aeronautical Research Council

1939–48 3*s.* (post 6*d.*) 1949–54 5*s.* (post 5*d.*)

Index to all Reports and Memoranda published in the Annual Technical Reports

1909–1947 R. & M. 2600 (out of print)

Indexes to the Reports and Memoranda of the Aeronautical Research Council

Between Nos. 2351–2449	R. & M. No. 2450 2*s.* (post 3*d.*)
Between Nos. 2451–2549	R. & M. No. 2550 2*s.* 6*d.* (post 3*d.*)
Between Nos. 2551–2649	R. & M. No. 2650 2*s.* 6*d.* (post 3*d.*)
Between Nos. 2651–2749	R. & M. No. 2750 2*s.* 6*d.* (post 3*d.*)
Between Nos. 2751–2849	R. & M. No. 2850 2*s.* 6*d.* (post 3*d.*)
Between Nos. 2851–2949	R. & M. No. 2950 3*s.* (post 3*d.*)
Between Nos. 2951–3049	R. & M. No. 3050 3*s.* 6*d.* (post 3*d.*)
Between Nos. 3051–3149	R. & M. No. 3150 3*s.* 6*d.* (post 3*d.*)

HER MAJESTY'S STATIONERY OFFICE

from the addresses overleaf

Printed and published by
HER MAJESTY'S STATIONERY OFFICE

To be purchased from
York House, Kingsway, London w.c.2
423 Oxford Street, London w.1
13A Castle Street, Edinburgh 2
109 St. Mary Street, Cardiff
39 King Street, Manchester 2
50 Fairfax Street, Bristol 1
35 Smallbrook, Ringway, Birmingham 5
80 Chichester Street, Belfast 1
or through any bookseller

Printed in England

S.O. Code No. 23-3381